

# RSC Advances



This is an *Accepted Manuscript*, which has been through the Royal Society of Chemistry peer review process and has been accepted for publication.

*Accepted Manuscripts* are published online shortly after acceptance, before technical editing, formatting and proof reading. Using this free service, authors can make their results available to the community, in citable form, before we publish the edited article. This *Accepted Manuscript* will be replaced by the edited, formatted and paginated article as soon as this is available.

You can find more information about *Accepted Manuscripts* in the [Information for Authors](#).

Please note that technical editing may introduce minor changes to the text and/or graphics, which may alter content. The journal's standard [Terms & Conditions](#) and the [Ethical guidelines](#) still apply. In no event shall the Royal Society of Chemistry be held responsible for any errors or omissions in this *Accepted Manuscript* or any consequences arising from the use of any information it contains.



## RSC advances

## ARTICLE

## Synergistic inhibition of carbon steel corrosion in 0.5 M HCl solution by indigo carmine and some cationic organic compounds: Experimental and Theoretical Studies

Received 00th January 20xx,  
Accepted 00th January 20xx

DOI: 10.1039/x0xx00000x

www.rsc.org/

Z. Zhang<sup>a, b</sup>, N. C. Tian<sup>a</sup>, X. D. Huang<sup>a</sup>, W. Shang<sup>a</sup>, L. Wu<sup>c</sup>

A synergistic inhibition effect between indigo carmine and three kinds of cationic organic compounds on 1045 carbon steel (CS) corroded in 0.5 M HCl solution is reported. The electrochemical measurements showed that these three cationic organic compounds combined with indigo carmine reduce the speed of corrosion on 1045 CS and act as an effective inhibitor. The indigo carmine with BAB had the best synergistic inhibition effect on corrosion ( $S=17.14$ ), and the best inhibition efficiency 95.0%. The SEM images and XPS data of the corroded iron surfaces suggested that the indigo disulphonate anion and organic cation could be simultaneously adsorbed on the CS surface to [pinhibit the corrosion of iron. The synergistic inhibition mechanism was investigated by dynamic simulations using quantum chemistry.

### 1. Introduction

As the a major construction materials, carbon steel is used extensively in various industrial environment. The corrosion of carbon steel usually is inevitable, and it leads to economic loss and personal injury<sup>[1,2]</sup>. Organic corrosion inhibitors are the best choice to protect the metals from corrosion due to the high efficiency, the low cost and “environmental- friendly”<sup>[3, 4]</sup>. Indigo dye is a traditional and natural compounds which have colour and be capable of imparting the colour to other materials on a reasonably permanent basis<sup>[5]</sup>. This nature will mean that the adsorption capability of indigo dye molecule is strong enough. Also, indigo dye and some other dyes have been reported to reduce and inhibit metal corrosion<sup>[5-10]</sup>.

As a derivative of the indigo molecule, indigo carmine molecule is considered as a candidate of indigo dye inhibitor for the better solubility. As shown in Table 1, indigo carmine molecule contains some N, O, S atoms and conjugates aromatic nucleus which suggest this molecule to be an efficient inhibitor. M. Abdeli et al<sup>[11]</sup>, reported that the indigo carmine could inhibit the mild steel from corrosion in 1 mol.L<sup>-1</sup> (M) HCl solution. The inhibition efficiency increased with small addition of indigo carmine and then

decreased when the concentration of indigo carmine was higher than  $9.65 \times 10^{-5}$  M. But, we found that the inhibition effect of indigo carmine is different on mild steel and 1045 carbon steel. The 1045 carbon steel could be accelerated corrosion while the concentration of indigo carmine reached above  $1 \times 10^{-4}$  M in our previous research<sup>[12]</sup>. The carbon content and the purity of the iron are important factors for the corrosion-resistance of carbon steel, which is weakened as the carbon content increases because the existence of carbon elements can enhance the electrochemical corrosion of carbon steel in a non-oxidizing acid medium<sup>[13-16]</sup>.

Consequently, the aim of the present work is to further verify the synergistic corrosion inhibition mechanism of indigo carmine and three kinds of cationic organic compounds for CS in 0.5 M HCl solution. Triethanolamine, Benzyl trimethyl ammonium bromide and Cetyl trimethyl ammonium bromide were selected as cationic organic compounds to eliminate the influence of hydrophobic property, and the structural formulas were shown in Table 1. Electrochemical measurements were used to study the inhibition efficiency of each inhibitors. XPS and SEM techniques were used to examine the surface morphology of CS sheets with and without inhibitors in the 0.5 M HCl solution for 48 h. The synergistic corrosion inhibition mechanism and the correlation between molecular structure and inhibition efficiency were investigated by molecular dynamic simulation and quantum chemical calculation.

### 2. Experiments

#### 2.1. Preparation of electrodes

1045 carbon steel (CS) specimens of composition (wt%) was C (0.45%), Si (0.17%), Mn (0.5%), S (0.035%), P (0.035%), Cr (0.25%), Cu (0.25%), Ni (0.30%), Fe (the remaining 98%). The preparation and preliminary process of CS working electrode (WE) referenced from the published article of Zhe Zhang, et al<sup>[12, 17]</sup>.

<sup>a</sup> Guangxi Key Laboratory of Electrochemical and Magneto-chemical Functional Materials, College of Chemistry and Bioengineering, Guilin University of Technology, Guilin 541004, PR China.

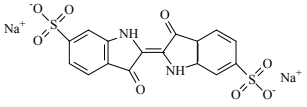
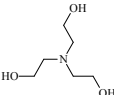
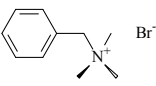
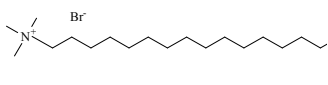
<sup>b</sup> Department of Chemical Engineering, Mid Sweden University, Sundsvall SE-85170, Sweden.

<sup>c</sup> School of Chemistry and Chemical Engineering, Shandong University, Jinan 250100, PR China.

† Footnotes relating to the title and/or authors should appear here.

Electronic Supplementary Information (ESI) available: [details of any supplementary information available should be included here]. See DOI: 10.1039/x0xx00000x

Table 1 The structural formulas and symbols of inhibitor molecules

Inhibitors	Structure	Symbol
Indigo carmine		--
Triethanolamine		TEA
Benzyl trimethyl ammonium bromide		BAB
Cetyl trimethyl ammonium bromide		CTAB

## 2.2. Formation of synergistic inhibitors solution

The indigo carmine ( $\cong 96\%$ , Aladdin Industrial Corporation) was dissolved in 0.5 M HCl solution, which was prepared from analytical-grade HCl (12 M) and ultra pure water at 25 °C. Then, the TEA ( $\cong 98\%$ , Aladdin Industrial Corporation), BAB ( $\cong 98\%$ , Aladdin Industrial Corporation) and CTAB ( $\cong 98\%$ , Aladdin Industrial Corporation) were dissolved in the indigo carmine solution under mechanically stirring, respectively. The molar ratio between indigo carmine and cationic organic compounds was 1: 2 in all the experiments. Finally, the obtained inhibition solution was allowed to stand for 2 h for the interaction of indigo carmine and CTAB at a room temperature of 25 °C.

## 2.3. Electrochemical measurements

In this study, the electrochemical measurements were performed by electrochemical impedance spectroscopy (EIS) and potentiodynamic polarization curves measurements, and the detail of experiments referenced from the published article of Zhe Zhang [12].

## 2.4. Surface observation and characterization

Specimen for characterization experiments were bare CS sheets (3 mm  $\times$  3 mm  $\times$  1 mm). The preliminary process was the same as chapter 2.1. After immersion for 48 h in 0.5 M HCl test solution which in the absence and presence of inhibitors, the CS sheets were rinsed with ultra pure water, and then vacuum dried in anhydrous ethanol at 50 °C. The surface characteristics of CS specimens were examined by scanning electron microscopy (SEM) Table 2 The details setup of molecular dynamics simulation

Basic setup	Method	Convergence Level	Maximum iteration	
	smart minimizer	ultra-fine	20000	
Minimizer setup	forcefield	non-nond	Summation method	Cutoff distance
	comoaass	vdW	Atom based	9.5 Å
Dynamic simulation setup	Ensemble	Thermostat	Simulation temperature	Energy deviation
	NVT	Andersen	298.0 K	5000.0 kcal/mol
	Dynamics time	Time step	Frame output	
	2000.0ps	1 fs	Every 1000 steps	

(JSM-6380LV). The XPS analysis of the corrosion surface was performed by X-ray photoelectron spectrometer (ESCALAB 250Xi system. Thermo Electron Corporation, USA) and the specimen was irradiated with Al K $\alpha$  radiation (photoelectron energy 1253.6 eV). Survey scans and relevant core levels were recorded: Fe 2p, C 1s, N 1s, O 1s and S 2p.

## 2.5. Quantum chemical calculations and dynamic simulations

In order to investigate the quantum chemical property of indigo carmine and other three kinds of cationic organic compounds, Gaussian 03W software [18] was used to perform the quantum chemical calculations. Geometrical optimization and the energy calculation were carried out with the Density Functional Theory (DFT) method of the Becke-type three-parameter hybrid combined with the gradient-corrected correlation function of Lee, Yang, and Parr (B3LYP) in conjunction with the 6-311G (d,p) basis set [19-21].

The adsorption configuration of indigo carmine molecule and other three kinds of cationic organic compound molecules on iron surface were dynamic simulated by using the Discover module of the Materials Studio 6.0 software from Accelrys Inc. [22]. The details setup of this molecular dynamic simulation were listed on Table 2. The detail of simulation system building process referenced from the published article of Zhe Zhang [12].

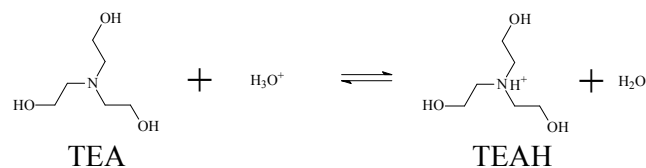


Fig. 1. The protonation process of TEA molecule in acidic solution.

The inhibitors aqueous solution layer and the confined water molecule layer which were constructed using the Amorphous Cell module contained 5 H<sub>3</sub>O<sup>+</sup> ions, 5 Cl<sup>-</sup> ions, 500 H<sub>2</sub>O molecules, 1 inhibitor molecule or 2 compounded inhibitor molecules and some corresponding inorganic ions in this simulated system to simulate the 0.5 M HCl solution. Due to the high tendency of TEA molecules be protonated in an acidic solution [17, 23-25], the TEAH was to be considered as a cationic organic compound in dynamic simulation, and the protonated process is shown in Fig. 1. In order to study the interaction between the inhibitors and Fe (1 1 0) surface, 6 layers iron atoms near the bottom were frozen. Before the molecular dynamic simulation, the constructed box could be optimized such that the total energy of the system was at a local minimum with respect to potential energy. Finally, the dynamic simulated process was carried out until both the temperature and the energy of the whole system reached equilibrium.

## RSC advances

## ARTICLE

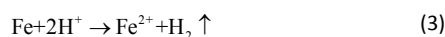
## 3. Results and discussion

## 3.1. Mechanism analysis of anti-corrosion and synergistic effect

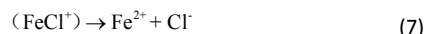
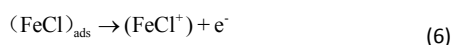
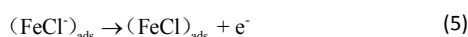
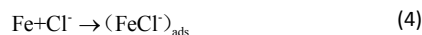
For the corrosion of carbon steel in HCl solution (while  $\text{pH} < 3$ ) the anodic (metal dissolution) and cathodic (hydrogen evolution) half reactions are [26-29]:



And the overall corrosion reaction equation showed as following:



The anodic dissolution of iron occurs according to the following step [30]:



In additionally, the hydrogen production occurs via two successive elementary events: firstly, the initial discharge of hydrogen ions to adsorbed monoatomic hydrogen [31]:



Followed by the chemical (Eq.9) or electrochemical (Eq.10) recombination of monoatomic hydrogen to molecular hydrogen.



To investigate the inhibition behavior of indigo carmine and other inhibitors (such as: various cationic organic inhibitors and various composite inhibitors) of CS in 0.5 M HCl solution at 25 °C, EIS and potentiodynamic polarization measurements were carried out. The Nyquist plots and polarization curves of WE measured in various test solutions were shown in Fig. 2, Fig. 3 and Fig. 4. We could find that all the Nyquist curves were shown as a single capacitive arc, which meant one time constant contained in these Nyquist plots. And, these capacitive arc were compressed type which could be attributed to the heterogeneity or roughness of WE surface [32]. In additionally, the Nyquist curves shape of all the test inhibitors were similar with the blank solution. That indicated the corrosion mechanism was almost no change whether the inhibitors were added [33].

Thus, the EIS data could be simulated by ZView2 software with a simple equivalent circuit  $R_s(\text{CPE}, R_{\text{ct}})$  and the fitting model shows

on Fig. 5. The fitting data are shown in Table 3. In this equivalent circuit,  $R_s$  represents the solution resistance between WE and SCE, and  $R_{\text{ct}}$  represents the charge-transfer resistance. For more accurately fitting the EIS of this study, *CPE* is constant phase element to replace a double layer capacitance ( $C_{\text{dl}}$ ), and the admittance and impedance of the *CPE* can be defined from the following formula [34, 35]:

$$Y_{\text{CPE}} = Y_0 (j\omega)^n \quad \text{and} \quad Z_{\text{CPE}} = \frac{1}{Y_0} (j\omega)^{-n} \quad (11)$$

where  $Y_0$  is the frequency independent parameters,  $n$  is the deviation parameter and  $\omega$  is the angular frequency. Accordingly, the values of  $C_{\text{dl}}$  can be calculated using Eq. (12) [36-38]:

$$C_{\text{dl}} = Y_0^{1/n} R_{\text{ct}}^{(1-n)/n} \quad (12)$$

where  $Y_0$  and  $n$  are the magnitude of the *CPE* and the deviation parameter, respectively.

The corrosion inhibition efficiencies ( $\eta_{\text{R}}$ ) of impedance have been estimated by  $R_{\text{ct}}$  according to the following formula:

$$\eta_{\text{R}}(\%) = \frac{R_{\text{ct}} - R_{\text{ct}}^0}{R_{\text{ct}}} \times 100 \quad (13)$$

where  $R_{\text{ct}}^0$  and  $R_{\text{ct}}$  are the charge transfer resistance of WE measured in the 0.5 M HCl solution and the 0.5 M HCl solution containing inhibitors, respectively.

In addition, The polarization curves for WE were measured and the results are shown in Fig. 2, Fig. 3 and Fig. 4. The polarization parameters which fitting using the built-in CHI760e software were listed on Table 4, such as: the corrosion potential ( $E_{\text{corr}}$ ), the cathodic and anodic Tafel slopes  $\beta_{\text{c}}$  and  $\beta_{\text{a}}$  ( $\text{V}\cdot\text{dec}^{-1}$ ), and the corrosion current density ( $i_{\text{corr}}$ ). These values were obtained via processed polarization curves by Tafel extrapolation. And, the protection efficiencies ( $\eta_{\text{i}}$ ) of corrosion current density were calculated by the following Eq. (4) and the results were listed on Table 4:

$$\eta_{\text{i}}(\%) = 1 - \frac{i_{\text{corr}}}{i_{\text{corr}}^0} \times 100 \quad (14)$$

where  $i_{\text{corr}}^0$  and  $i_{\text{corr}}$  represent the corrosion current densities of WE in 0.5 M HCl and 0.5 M HCl containing inhibitors, respectively.

## 3.1.1 Corrosion inhibition mechanism of indigo carmine

From Fig. 2a and Table 3, the  $R_{\text{ct}}$  values of indigo carmine increased with the concentration increasing at a small addition, which indicated a concentration-dependent increased of the protection efficiency at low concentration. While the concentration of indigo carmine above  $5 \times 10^{-5}$  M, the  $R_{\text{ct}}$  of indigo carmine decreased with the concentration increasing. Due to the indigo carmine molecules existed in HCl solution as indigo disulphonate ion and sodium ion, this phenomenon could be explained as



following: the indigo disulphonate ion was adsorbed on the CS surface with hardly changing the charge distribution of CS at tiny concentration, and the adsorbed indigo disulphonate ion have covered on the some active sites of CS to reduce the corrosion of iron by HCl solution; While the concentration of indigo carmine increasing, more and more indigo disulphonate ions were adsorbed on active sites of the CS surface and then the charge distribution of CS changed to a negatively charged surface which would gather the

$H^+$  ions on WE surface. An increase in concentration of  $H^+$  ions promote the corrosion reaction of iron in HCl solution (see as Eq. 3), then induce the  $H^+$  discharging and accelerate corrosion<sup>[31, 39, 40]</sup>. So, we could draw a conclusion that the indigo disulphonate ion could adsorb strongly on CS surface through nitrogen atoms, sulfur atoms and oxygen atoms, but it was disabled to protect the iron from corrosion due to the negatively charged surface<sup>[12]</sup>.

Table 3 Impedance parameters of WE measured in 0.5 M HCl solution with various inhibitors containing

Inhibitors	Concentration (mol.L <sup>-1</sup> )	Molar ratio	$R_s$ ( $\Omega$ )	CPE		$C_{dl}$ ( $\mu Fcm^{-2}$ )	$R_{ct}$ ( $\Omega cm^{-2}$ )	$\eta_R$ (%)
				$Y_0(\mu\Omega^{-1}S^n cm^{-2})$	n			
Blank sample	0	--	6.98	27.77	0.852	9.47	74.0	--
Indigo	0.00001	--	6.29	71.17	0.818	24.18	111.0	33.3
	0.00005	--	6.78	77.51	0.830	26.39	68.2	-8.5
	0.0001	--	6.83	97.66	0.831	34.35	60.5	-22.4
	0.0005	--	6.23	160.69	0.829	58.42	46.2	-60.3
	0.001	--	6.93	256.32	0.804	84.57	41.6	-78.0
	0.005	--	6.63	268.25	0.806	84.58	31.0	-138.9
	0.01	--	6.22	424.13	0.791	126.70	24.5	-202.7
TEA	0.0002	--	6.76	263.43	0.809	83.77	29.5	-151.2
	0.001	--	7.05	210.00	0.808	64.00	31.6	-134.4
	0.002	--	7.22	179.32	0.834	69.21	46.0	-61.0
	0.01	--	6.65	78.43	0.835	29.81	94.2	21.4
	0.02	--	6.66	83.16	0.837	34.10	122.0	39.3
BAB	0.0002	--	6.63	256.32	0.804	78.70	31.0	-138.9
	0.001	--	6.78	199.46	0.824	72.66	44.5	-66.1
	0.002	--	6.71	144.68	0.833	55.00	55.1	-34.2
	0.01	--	6.50	44.37	0.865	20.42	159.5	53.6
	0.02	--	6.72	47.64	0.838	19.34	195.3	62.1
CTAB	0.00002	--	6.78	18.08	0.753	4.92	1055.0	93.0
	0.0001	--	6.60	12.59	0.791	4.73	1938.0	96.2
	0.0002	--	5.68	11.59	0.875	7.01	2527.0	97.1
	0.001	--	6.43	12.09	0.820	5.36	2046.0	96.4
	Indigo/TEA	0.0001	1:2	7.58	115.49	0.826	43.92	89.1
0.0005		1:2	6.92	44.10	0.848	18.42	172.6	57.1
0.001		1:2	6.33	28.29	0.832	10.44	250.9	70.5
0.005		1:2	7.00	25.87	0.854	11.37	313.8	76.4
0.01		1:2	6.65	44.76	0.860	20.53	189.1	60.9
Indigo/BAB	0.0001	1:2	6.61	41.79	0.817	13.96	179.3	58.7
	0.0005	1:2	6.68	29.07	0.835	13.06	594.9	87.6
	0.001	1:2	6.48	35.26	0.780	13.24	884.0	91.6
	0.005	1:2	6.19	31.55	0.823	15.91	1301.0	94.3
	0.01	1:2	6.50	27.98	0.825	14.37	1546.0	95.2
Indigo/CTAB	0.00001	1:2	6.51	7.88	0.810	2.73	1399.0	94.7
	0.00005	1:2	6.74	9.48	0.779	3.85	4387.0	98.3
	0.0001	1:2	6.69	7.71	0.791	2.92	3290.0	97.8
	0.0005	1:2	6.52	8.43	0.805	3.19	2177.0	96.6

On Table 3, the  $C_{dl}$  of indigo carmine increased from 9.49 to 126.70  $\mu\text{F}\cdot\text{cm}^{-2}$  with the concentration increased. According to the Helmholtz model, this result is reasonable in which  $C_{dl}$  is inversely proportional to the surface changes and directly proportional to the local dielectric constant of WE surface<sup>[37, 41, 42]</sup>.

$$C_{dl} = \frac{\epsilon_0 \epsilon A}{d} \quad (15)$$

where  $A$  is the electrode surface,  $d$  is the film thickness,  $\epsilon_0$  is the permittivity of air, and  $\epsilon$  is the local dielectric constant. The increase in the  $C_{dl}$  value is attributed to the replacement of the adsorbed water molecules at the WE surface by the indigo disulphonate ion that have a higher dielectric constant<sup>[43]</sup>. These points suggest that the local dielectric constant of WE was changed by indigo disulphonate ion adsorption at the metal–solution interface, thereby increasing the  $C_{dl}$  value. It is inferred that the adsorption quantity of indigo disulphonate ion increased with the concentration of indigo carmine increasing at same immersion time. Also, the large increasing of  $C_{dl}$  may be because of the loose and porous corrosion products (equal a porous electrode surface which  $C_{dl}$  is very high) have covered on WE surface. It means that the corrosion degree of 0.5 M HCl solution with indigo carmine is more serious with the concentration increasing at same immersion time.

The  $n$  values on Table 3 are changed from 0.852 to 0.791 with obvious regularity. The reason may be that the surface of WE is non-homogeneous, and the surface quality was become worse due to the accelerating corrosion of the indigo carmine in 0.5 M HCl solution.

From Fig. 2b, we can find that the anodic and cathodic current densities all changed with the concentration increasing. Except the corrosion current densities of the  $1 \times 10^{-5}$  M indigo carmine sample

was less than the blank sample, the  $i_{corr}$  of indigo carmine samples increased with the concentration increasing and higher than blank sample (on Table 4). It mean the indigo carmine could inhibited the corrosion of CS in 0.5 M HCl solution with the concentration about  $1 \times 10^{-5}$  M. While the concentration of indigo carmine above  $5 \times 10^{-5}$  M, the indigo carmine could accelerate the corrosion of CS in 0.5 M HCl solution. Comparing the cathodic and anodic Tafel slopes  $\beta_c$  and  $\beta_a$  of indigo carmine on Table 4, we can found that the increasing of  $\beta_c$  are bigger than the increasing of  $\beta_a$ , which means the hydrogen reduction in the cathodic region are further accelerated. This indicated that the adsorbed indigo disulphonate ion inducing the  $\text{H}^+$  discharging on CS surface is the major factor of the indigo carmine accelerating the CS corrosion in 0.5 M HCl solution.

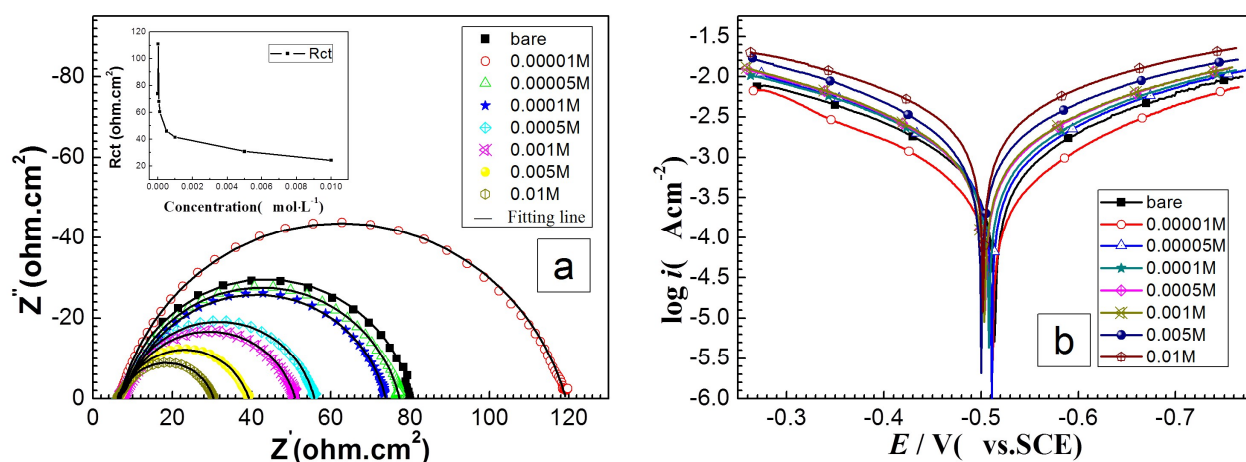


Fig. 2. Nyquist impedance spectra and potentiodynamic polarization curves of WE measured in 0.5 M HCl solutions which contains indigo carmine inhibitors. The solid lines are their fitted curves in the impedance spectra.

### 3.1.2 Inhibition mechanism of cationic organic inhibitors

On Table 3 the  $R_{ct}$  values of TEA and BAB samples were lower than that of blank sample when the concentration was under 0.01 M. While the concentration was above 0.01 M, the  $R_{ct}$  of TEA and BAB samples were higher than the  $R_{ct}$  of blank sample. And, the  $R_{ct}$  of TEA and BAB samples all increased with the concentration increasing. This phenomenon indicated the TEA and BAB could not inhibit the corrosion of CS in 0.5 M HCl solution, on the contrary, the TEA and BAB could accelerate the corrosion with the lower concentration. Due to the protonation of TEA and the hydrolysis of BAB, the TEA and BAB could exist in HCl solution as TEAH, benzyl trimethyl ammonium ion and bromide ion. The reason may be that the adsorption of TEAH or benzyl trimethyl ammonium ion on CS surface could change the charge distribution of CS from zero charge to be positively charged which would gather the  $\text{Cl}^-$  ions on the CS surface and corrode the iron surface with pitting corrosion. While

the concentration of TEA and BAB was above 0.01 M, more and more TEAH or benzyl trimethyl ammonium ions could be adsorbed on CS surface, gradually, a dense film formed. Although,  $\text{Cl}^-$  ions were gathered on the CS surface, this dense film could isolate the  $\text{Cl}^-$  ions and inhibit the pitting corrosion. From Fig. 3e or Table 3, we could find all the  $R_{ct}$  of CTAB are higher than that of the blank sample. And the  $R_{ct}$  of CTAB increased with the concentration increasing when the concentration of CTAB was less than 0.0002 M. While the concentration of CTAB was above 0.0002 M, the  $R_{ct}$  of CTAB decreased with the concentration increasing. It indicated the CTAB could effectively inhibit the corrosion of CS in 0.5 M HCl solution. That may be because of the molecular structure of CTAB contained a long-chain alkyl group which could make the adsorbed cetyl trimethyl ammonium ion arrange on CS surface one by one and form a hydrophobic layers to protect CS from corrosion. Due to the agglomeration phenomena of a long-chain alkyl molecule, the

## ARTICLE

## RSC advances

$\eta_R$  of CTAB decreased when the concentration of CTAB was above 0.0002 M.

From the  $C_{dl}$  of this three kinds of cationic organic inhibitors, we could find the  $C_{dl}$  of them follow in the order of TEA > BAB >> CTAB. The  $C_{dl}$  of TEA and BAB was a little difference, but both were higher than the  $C_{dl}$  of CTAB. Especially, the  $C_{dl}$  of CTAB all were lower than that of the blank sample. The local dielectric constant ( $\epsilon$ ) of the CS surface which adsorbed TEAH or benzyl trimethyl ammonium ion was much higher than the  $\epsilon$  of the CS surface which adsorbed cetyl trimethyl ammonium ion due to the hydrophobicity

of cetyl trimethyl ammonium ion is better than TEAH and benzyl trimethyl ammonium ion. From the values of  $n$  on Table 3, we could find the  $n$  of each cationic organic inhibitors increased in the range of 0.8 to 0.9 with the concentration increasing. The reason may be that the surface of working electrodes is non-homogeneous, and the self-assembled films improve the heterogeneity. In summary, this three kinds of cationic organic inhibitors all can became adsorbed on CS surface and form a film with different properties, the corrosion inhibition effect of them follow the order of CTAB >> BAB > TEA.

Table 4 Polarization parameters for the WE measured in 0.5 M HCl solutions with various inhibitors containing

inhibitors	concentration (mol.L <sup>-1</sup> )	Molar ratio	$E_{corr}$ (V vs. SCE)	$-\beta_c$ (V dec <sup>-1</sup> )	$\beta_a$ (V dec <sup>-1</sup> )	$i_{corr}$ ( $\mu$ A cm <sup>-2</sup> )	$\eta_l$ (%)	S
Blank sample	0	--	-0.515	0.157	0.165	664.6	--	--
Indigo	0.00001	--	-0.513	0.153	0.157	373.2	43.8	--
	0.00005	--	-0.511	0.154	0.157	765.5	-15.2	--
	0.0001	--	-0.508	0.160	0.165	877.1	-32.0	--
	0.0005	--	-0.504	0.163	0.169	994.0	-49.6	--
	0.001	--	-0.503	0.162	0.164	1025.0	-54.2	--
	0.005	--	-0.501	0.170	0.163	1462.0	-120.0	--
	0.01	--	-0.502	0.183	0.192	2694.0	-305.4	--
TEA	0.0002	--	-0.506	0.172	0.175	1451.0	-118.3	--
	0.001	--	-0.504	0.173	0.172	1386.0	-108.5	--
	0.002	--	-0.506	0.163	0.163	1037.0	-56.0	--
	0.01	--	-0.509	0.147	0.145	472.9	28.8	--
	0.02	--	-0.509	0.143	0.142	437.5	34.2	--
BAB	0.0002	--	-0.501	0.170	0.164	1462.0	-120.0	--
	0.001	--	-0.502	0.165	0.161	1008.0	-51.7	--
	0.002	--	-0.504	0.155	0.148	798.1	-20.1	--
	0.01	--	-0.503	0.147	0.140	367.1	44.8	--
	0.02	--	-0.505	0.145	0.132	280.2	57.8	--
CTAB	0.00002	--	-0.525	0.158	0.150	51.7	92.2	--
	0.0001	--	-0.524	0.155	0.145	24.0	96.4	--
	0.0002	--	-0.524	0.148	0.120	16.4	97.5	--
	0.001	--	-0.528	0.156	0.128	18.4	97.2	--
Indigo/TEA	0.0001	1:2	-0.512	0.146	0.147	478.9	27.9	4.00
	0.0005	1:2	-0.513	0.143	0.146	349.8	47.4	5.93
	0.001	1:2	-0.524	0.188	0.160	185.8	72.0	8.61
	0.005	1:2	-0.522	0.190	0.161	176.2	73.5	5.90
	0.01	1:2	-0.523	0.182	0.164	240.4	63.8	7.38
Indigo/BAB	0.0001	1:2	-0.511	0.141	0.130	286.9	56.8	15.79
	0.0005	1:2	-0.512	0.133	0.114	80.4	87.9	17.14
	0.001	1:2	-0.523	0.125	0.098	56.7	91.5	16.31
	0.005	1:2	-0.522	0.117	0.090	42.5	93.6	12.03
	0.01	1:2	-0.523	0.118	0.091	33.2	95.0	12.44
Indigo/CTAB	0.00001	1:2	-0.521	0.157	0.134	30.9	95.3	0.94
	0.00005	1:2	-0.523	0.142	0.109	9.9	98.5	3.63
	0.0001	1:2	-0.524	0.139	0.112	13.2	98.0	1.92
	0.0005	1:2	-0.520	0.150	0.109	21.8	96.7	1.86

## RSC advances

## ARTICLE

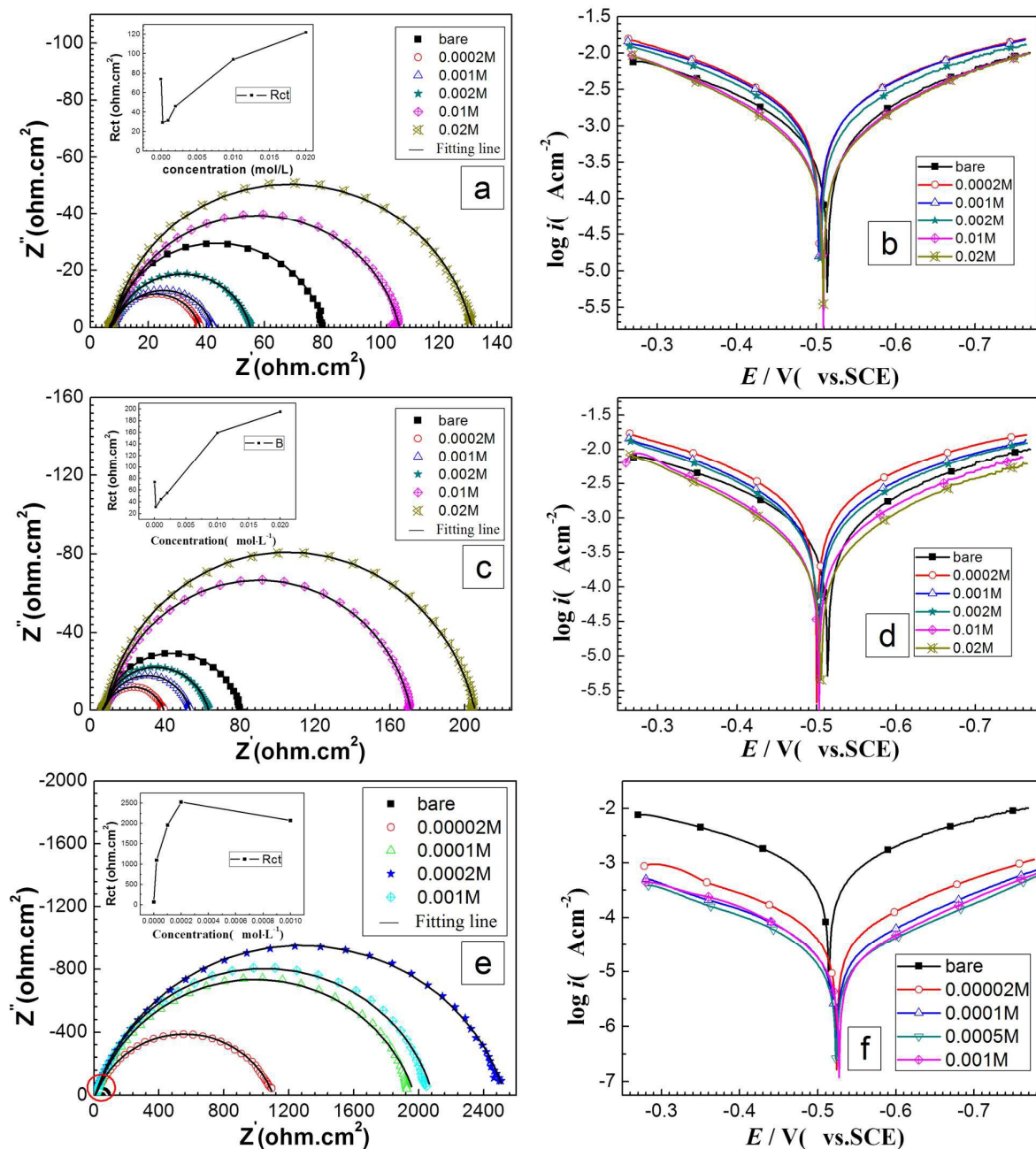


Fig. 3. Nyquist impedance spectra and Potentiodynamic polarization curves of WE measured in 0.5 M HCl solutions which contains various cationic organic inhibitors. TEA: (a) and (b), BAB: (c) and (d), CTAB: (e) and (f). The solid lines are their fitted curves in the impedance spectra.

## RSC advances

## ARTICLE

On Table 4, we can find the  $i_{\text{corr}}$  of TEA and BAB were higher than blank sample when concentration under 0.01 M. When the concentration of TEA and BAB above 0.01 M, the  $i_{\text{corr}}$  of them were lower than blank sample. And the  $i_{\text{corr}}$  of them were decreased with the concentration increasing. It means that the TEA and BAB could inhibit the corrosion of CS in 0.5 M HCl solution while the concentration is high enough. The  $i_{\text{corr}}$  of CTAB were all lower than that of the blank sample which indicated CTAB could effectively inhibit the CS from corrosion. These results are consistent with the result from EIS measurements. From the polarization curves in Fig. 3, we could find the anodic and cathodic current densities obviously decreased while these three kinds of cationic organic inhibitors play a inhibitor role. This oxidative dissolution of the working electrodes in the anodic region and hydrogen reduction in the cathodic region were weaker in the Tafel plots, which indicated that the anodic dissolution of CS and hydrogen evolution were both suppressed. In general, the inhibitors can be classified as an anodic or cathodic types when the change in  $E_{\text{corr}}$  value is greater than 85 mV<sup>[44-47]</sup>. Obviously, the TEA and BAB could be classified as mixed type inhibitors due to the  $E_{\text{corr}}$  of them shift slightly. Although, the  $E_{\text{corr}}$  of CTAB all shifted toward to negative, but the maximal displacement was also less than 85 mV. So, the CTAB also can be classified as a mixed type inhibitor.

### 3.1.3 Inhibition mechanism of the compound inhibitors

The Nyquist impedance plots of CS in the absence and presence of various compound inhibitors are plotted in Fig. 4. The intercept of each capacitive loops on the horizontal axis were bigger than that of the blank sample. It indicated that this three kinds of compound inhibitors all could inhibit the CS from corrosion in 0.5 M HCl solution, and the most  $R_{\text{ct}}$  of them increased with the concentration increasing. Comparing with the  $R_{\text{ct}}$  of indigo carmine and another three kinds of cationic organic inhibitors, we can find the  $R_{\text{ct}}$  of these compound inhibitors were much higher than other single inhibitors at the same concentration. It meant that the indigo carmine combining with a kind of cationic organic inhibitors could improve its inhibition of CS in 0.5 M HCl solution. In additionally, we could find the  $R_{\text{ct}}$  of indigo camine/TEA and indigo carmine/CTAB were decreased with the concentration increasing when the concentration was high enough. For the indigo disulphonate anion and TEAH or cetyltrimethylammonium cation coexistence in 0.5 M HCl solution, this phenomenon could be explained as following: while the concentration of indigo carmine/TEA (or indigo carmine/CTAB) was lower, the indigo disulphonate anion and TEAH (or the indigo disulphonate anion and cetyltrimethylammonium cation) were adsorbed evenly on CS surface, gradually, a dense film formed; on the contrary, while the concentration of indigo carmine/TEA (or indigo carmine/CTAB) was higher, the indigo disulphonate anion and TEAH (or the indigo disulphonate anion and cetyltrimethylammonium cation) were competitively adsorbed on the CS surface and formed an unstable molecular film. Due to the molecular structure of BAB and indigo

carmine all contained some aromatic ring groups, the indigo carmine/BAB compound inhibitor was slightly affected by this competitively adsorption.

From Table 3, the  $C_{\text{dl}}$  of this three kinds of compound inhibitors were much smaller than the single indigo carmine or corresponding single cationic organic inhibitors. Especially, the  $C_{\text{dl}}$  of indigo carmine/CTAB were smaller than that of the blank sample. This result indicated the local dielectric constant of the CS surface modified with various compound inhibitors was decreased due to the indigo disulphonate anion and other organic cation simultaneously adsorb on CS surface to equilibrate the charge distribution of CS. The  $n$  of each compound inhibitors changed in the range of 0.78 to 0.86 with no obvious regularity in Table 3. It may because of that the surface heterogeneity of CS was changed with no obvious regularity due to the two oppositely charged molecules simultaneously adsorb on CS surface. But this change of  $n$  was acceptable. Thus, we inferred that the indigo carmine and the cationic organic inhibitors could adsorb simultaneously on CS surface, and formed a more stable and excellent film to protect CS from corrosion in 0.5 M HCl solution.

From the polarization curves in Fig. 4, we could find the anodic and cathodic current densities obviously decreased. And the  $i_{\text{corr}}$  of this three kinds of compound inhibitors, decreased with the concentration increasing in Table 4. The oxidative dissolution of the working electrodes in the anodic region and the hydrogen reduction in the cathodic region were both weaker in the Tafel plots, which indicated that the anodic dissolution of CS and hydrogen evolution were both suppressed. Besides the Tafel slopes  $\beta_c$  and  $\beta_a$  of indigo carmine/TEA increased with the concentration increasing, the Tafel slopes  $\beta_c$  and  $\beta_a$  of indigo carmine/BAB and indigo carmine/CTAB both decreased with the concentration increasing in Table 4. The reason may be that the adsorption capability of indigo carmine was stronger than TEA, thus, more and more TEA molecules could be replaced by indigo carmine molecules with the concentration increasing. So, the Tafel slopes change of indigo carmine/TEA was consistent with the Tafel slopes change of indigo carmine. In additionally, the change of  $\beta_a$  was more than  $\beta_c$  for both indigo carmine/BAB and indigo carmine/CTAB compound inhibitors, which indicted the anodic dissolution inhibiting was stronger than the hydrogen evolution inhibiting. However, in these experiments, the largest displacement of  $E_{\text{corr}}$  ( $\Delta E_{\text{corr}}$ ) was lower than 20 mV (vs. SCE, in Table 4). This displacement indicate that these three kinds of compound inhibitors all act as a mixed-type inhibitors by inhibiting both hydrogen evolution and the CS dissolution reaction. In summary, these three kinds of compound inhibitors could effectively inhibit the corrosion of CS in 0.5 M HCl solution, and the protection efficiencies of them followed in the order of indigo carmine/CTAB > indigo carmine/BAB > indigo carmine/TEA, the maximal protection efficiencies was 98.5% of indigo carmine/CTAB compound inhibitors.



## RSC advances

## ARTICLE

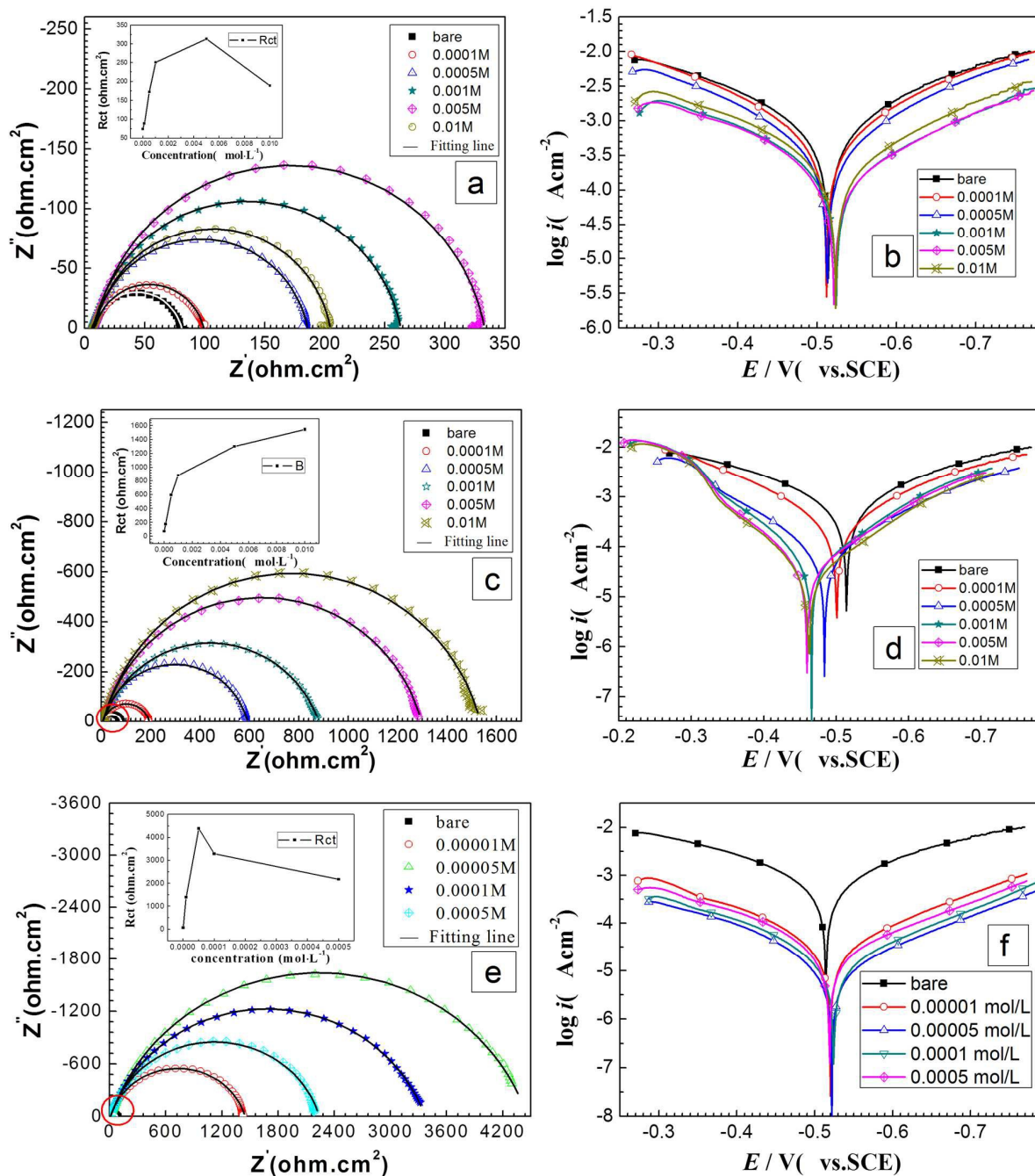


Fig. 4. Nyquist impedance spectra and Potentiodynamic polarization curves of WE measured in 0.5 M HCl solutions which contains various composite inhibitors. indigo carmine/TEA: (a) and (b), indigo carmine/BAB: (c) and (d), indigo carmine/CTAB: (e) and (f). The solid lines are their fitted curves in the impedance spectra.



## RSC advances

## ARTICLE

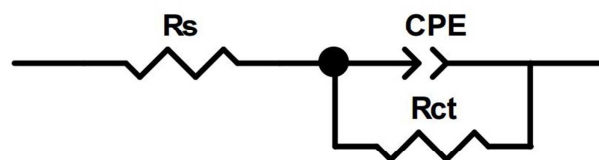


Fig. 5. Electrical equivalent circuit diagram used for modeling WE/solution interface in 0.5 M HCl solution.

### 3.1.4 Synergistic inhibition effect and the synergistic mechanism

From Fig. 2, Fig. 3, the single indigo carmine and other single cationic organic inhibitors were not an very well corrosion inhibitors in 0.5 M HCl solutions (except CTAB which hydrophobicity was very well). Especially, the single indigo carmine inhibitors and some low concentration of cationic organic inhibitors (such as: TEA and BAB) could lead an accelerated corrosion effect. The observed effect also correlated well to the potentiodynamic polarization measurements (Fig. 2 and Fig. 3). The compound inhibitors of indigo carmine/TEA, indigo carmine/BAB and indigo carmine/CTAB all decreased significantly the corrosion activity. Especially, the  $R_{ct}$  of indigo carmine/BAB was greatly improved relative to the single indigo carmine inhibitor and single BAB inhibitor. To effectively evaluate the synergistic inhibition, the synergistic parameter ( $S$ ) was calculated using the equation suggested by Aramaki and Hackerman [19, 48].

$$S = \frac{1 - \eta_{(1+2)}}{1 - \eta_{(1/2)}} \quad (16)$$

where  $\eta_{(1+2)} = (\eta_1 + \eta_2) - (\eta_1 \times \eta_2)$ .  $\eta_1$ ,  $\eta_2$  and  $\eta_{1/2}$ , are calculated from the protection efficiencies ( $\eta_i$ ) of the potentiodynamic polarization measurements for inhibitors indigo carmine, cationic organics and the compound inhibitors of indigo carmine/cationic organics. The  $S > 1$  indicate the synergistic behavior of selected inhibitor combination. The synergy factor of indigo carmine/BAB inhibitor which calculated from measured corrosion currents density is significantly above 1 ( $S = 17.14$ ) in this study. It demonstrate a high synergy between indigo carmine and BAB inhibitors. Comparing with the  $S$  of these three kinds of compound inhibitors, the synergistic inhibition effect followed in the order of: indigo carmine/BAB > indigo carmine/TEA > indigo carmine/CTAB (on Table 4). The low synergy between indigo carmine/CTAB compound inhibitor may because of that the hydrophobicity of CTAB was too well to conceal the synergy between indigo carmine and CTAB inhibitors.

In summary, the synergistic inhibition mechanism of the present work can be described as follow in:

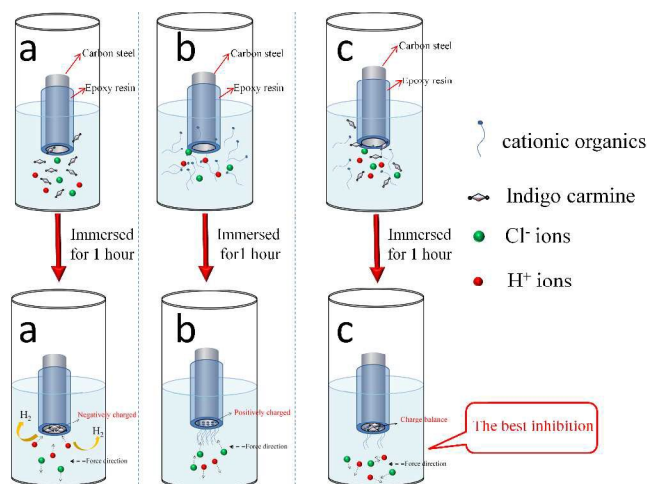


Fig. 6. Schematic mechanism of the synergistic effect by the combination of indigo carmine and cationic organics.

Firstly, the single indigo carmine could strongly adsorb on CS surface through nitrogen atoms, sulfur atoms, oxygen atoms and aromatic ring groups, but it was disabled to protect the iron from corrosion in 0.5 M HCl solution which because of the indigo disulphonate ions adsorbing on the CS surface could change the charge distribution of CS to be a negatively charged surface. This negatively charged surface would induce the  $H^+$  discharging and accelerate corrosion (as is shown in Fig.6a). Secondly, the single cationic organics could inhibit the corrosion of CS in 0.5 M HCl by forming a complete and dense adsorption film while the concentration was high enough (such as: CTAB could adsorb on iron surface with forming a dense hydrophobic film). If the cationic organics adsorption film was broken, the iron surface would be pitting corroded by  $Cl^-$  ions which  $Cl^-$  ions were gathered around the iron surface for the positively charged surface (as is shown in Fig. 6b). So that the single cationic organics could be described as "dangerous inhibitors". Finally, the indigo disulphonate ions and organic cationic ions could were adsorbed evenly on CS surface, gradually, a dense film formed when the indigo carmine combining with cationic organic. And this co-adsorption would not break the charge distribution of CS (as is shown in Fig. 6c). Thus, the inhibition effect of compound inhibitors are better than that of the single indigo carmine or other cationic organics inhibitors.

### 3.2. Surface morphological observation and analysis

The experimental results provided evidence that the corrosion inhibition of indigo compound inhibitors are pretty efficient. Immersion experiments were used to verify this results. The CS sheets had immersed in 0.5 M HCl solution and presence of indigo carmine, CTAB and indigo carmine/CTAB inhibitors, and the corrosion processes were showed in the corrosion process photograph (in Fig. 7). The CS sheets immersed in 0.5 M HCl solution and presence of indigo carmine inhibitors have turned

black for immersed 2 h which indicated the CS sheets were corroded. After immersed 48 h, these CS sheets have turned brown, and the solution have turned to be turbid which indicated the CS sheets were corroded badly and the dissolved iron have turn be

$\text{Fe}(\text{OH})_3$  (shown in Fig. 7b, and Fig. 7c). But the CS sheets immersed in 0.5 M HCl with presence of CTAB and indigo carmine/CTAB have hardly changed, and the surface of them were still bright (shown in Fig. 7h, and Fig. 7i).

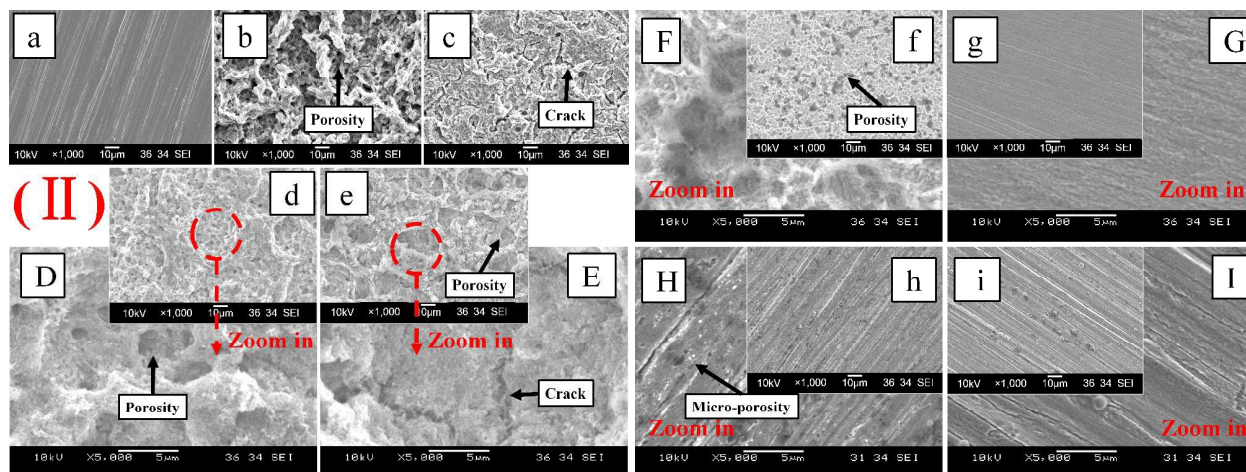
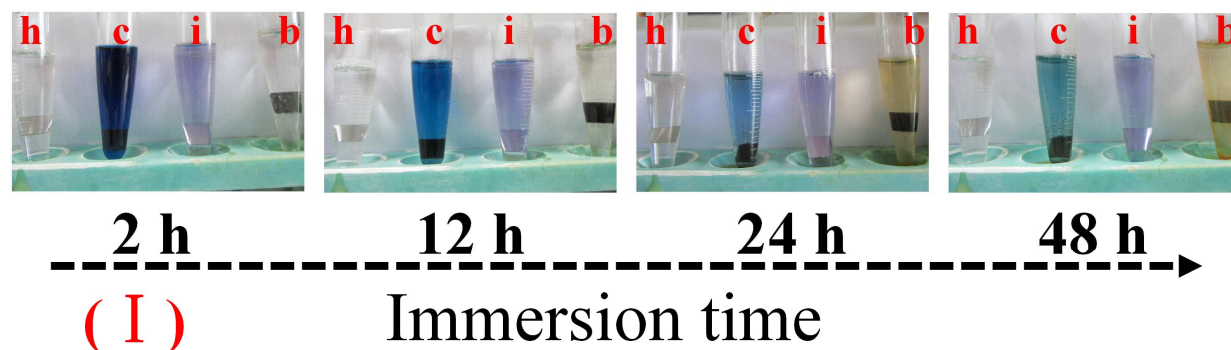


Fig. 7. The corrosion process photograph and SEM micrographs of corrosion surfaces formed by the CS sheets immersed in various test solution for 48 h: (a) CS sheet without immersing, (b) 0.5 M HCl, (c) 0.5 M HCl and presence of 0.0001 M indigo carmine, (d) 0.5 M HCl and presence of 0.01 M TEA, (e) 0.5 M HCl and presence of 0.02 M indigo carmine/TEA, (f) 0.5 M HCl and presence of 0.02 M BAB, (g) 0.5 M HCl and presence of 0.01 M indigo carmine/BAB, (h) 0.5 M HCl and presence of 0.0002 M CTAB, (i) 0.5 M HCl and presence of  $5 \times 10^{-5}$  M indigo carmine/CTAB, and the (D), (E), (F), (G), (H), (I) were the detail view of (d), (e), (f), (g), (h), (i), respectively.

The morphologies of CS surface immersed in the corrosion solution in the absence and presence of various inhibitors are displayed in SEM micrographs (on Fig. 7). It can be observed that the CS surface was corroded badly in the 0.5 M HCl solution (Fig. 7b). The porous structure was distributed on the corroded surface which the multi-hole may be caused by the  $\text{Cl}^-$  ions erosion process<sup>[28, 49]</sup>. In contrast, the more flat and cracked structure was shown on the CS surface which was corroded in 0.5 M HCl solution with containing indigo carmine (Fig. 7c). This cracked structure indicated this CS surface may be corroded by the hydrogen evolution reaction<sup>[50]</sup>. In addition, the corroded surface showed a network feature with a non-uniform distribution and irregularly micro-cracks, which means that the indigo disulphonate anion have been adsorbed on the CS surface and partly inhibited the corrosion. But the negatively charged surface induced the  $\text{H}^+$  discharging and caused hydrogen evolution reaction on uncovered area. It can be observed that the CS surface was pitting corroded in different degree in the 0.5 M HCl solution with containing TEA, BAB and CTAB, and the corrosion morphology all showed as porous structure (Fig. 7d, Fig. 7f and Fig. 7h). The damage of CS followed in the order of TEA > BAB > CTAB. But the damage of CS sheet immersed in BAB

or CTAB containing corrosion solution was better than that of the CS surface immersed in the 0.5 M HCl solution. That means the single cationic organic inhibitors (TEA, BAB and CTAB) could adsorb on CS surface and protect it from corrosion. But if the adsorption films of cationic organic inhibitors were not complete enough or broken, the CS could be pitting corroded in the cationic organic inhibitors containing corrosion solution. In contrast, the damage of CS sheets immersed in compound inhibitors containing corrosion solution were all better than the CS sheets immersed in single cationic organic inhibitors containing solution (Fig. 7e, Fig. 7g and Fig. 7i). Comparing with Fig. 7f and Fig. 7g, we could find that the pitting corrosion on CS surface was obviously inhibited by indigo carmine/BAB compound inhibitors. The inhibition effect of these three kinds of compound inhibitors followed in the order of: indigo carmine/CTAB > indigo carmine/BAB > indigo carmine/TEA from the surface morphology. This result is consistent with the electrochemical measurements.

### 3.3. the surface composition of corrosion surface

As XPS is a useful method for determining the composition of a surface<sup>[51, 52]</sup>, the corroded surface have been analyzed in this

study. The specimen of XPS spectra were the CS sheets which were immersed in indigo carmine/CTAB ( $5 \times 10^{-5}$  M) containing corrosion solution for 48 h. A wide-scan XPS spectrum of the test specimen were shown in Fig. 8a and confirmed the presence of the indigo carmine (such as: C, N, O and S) on the corrosion surface. To determine the different components of each high-resolution XPS spectrum, we have fitted the peaks of C, N, O, S and Fe element, and checked the elements of the energy of XPS from the data base<sup>[53, 54]</sup>. The peaks at 712.5 eV and 529.8 eV (on Fig. 8b and Fig. 8d) may be caused by the presence of some  $\text{Fe}^{3+}$  and  $\text{Fe}^{2+}$  on the CS surface or a certain degree of oxidation of Fe

that most likely occurred during the preparation process or part of iron atoms have been corroded during immersion process (Fig. 8b). The peaks at 712.5 eV and 168.3 eV of  $\text{Fe}_2(\text{SO}_4)_3$  (on Fig. 8b and Fig. 8f) indicated the indigo carmine molecules could adsorb on iron surface by chemisorptions (forming a coordinate bond). The peaks at 284.7 eV of C=O (Fig. 8c and Fig. 8d), 284.7 eV of aromatic rings (Fig. 8c) and 168.3 ~ 168.8 eV of sulfo groups (Fig. 8f) proved that the indigo carmine molecules had adsorbed on CS surface. In addition, the peaks at 400.4 eV of  $\text{NH}_4^+$  (Fig. 8e) and 285.7 eV of C-N (Fig. 8c) confirmed the presence of the CTAB molecules on CS surface.

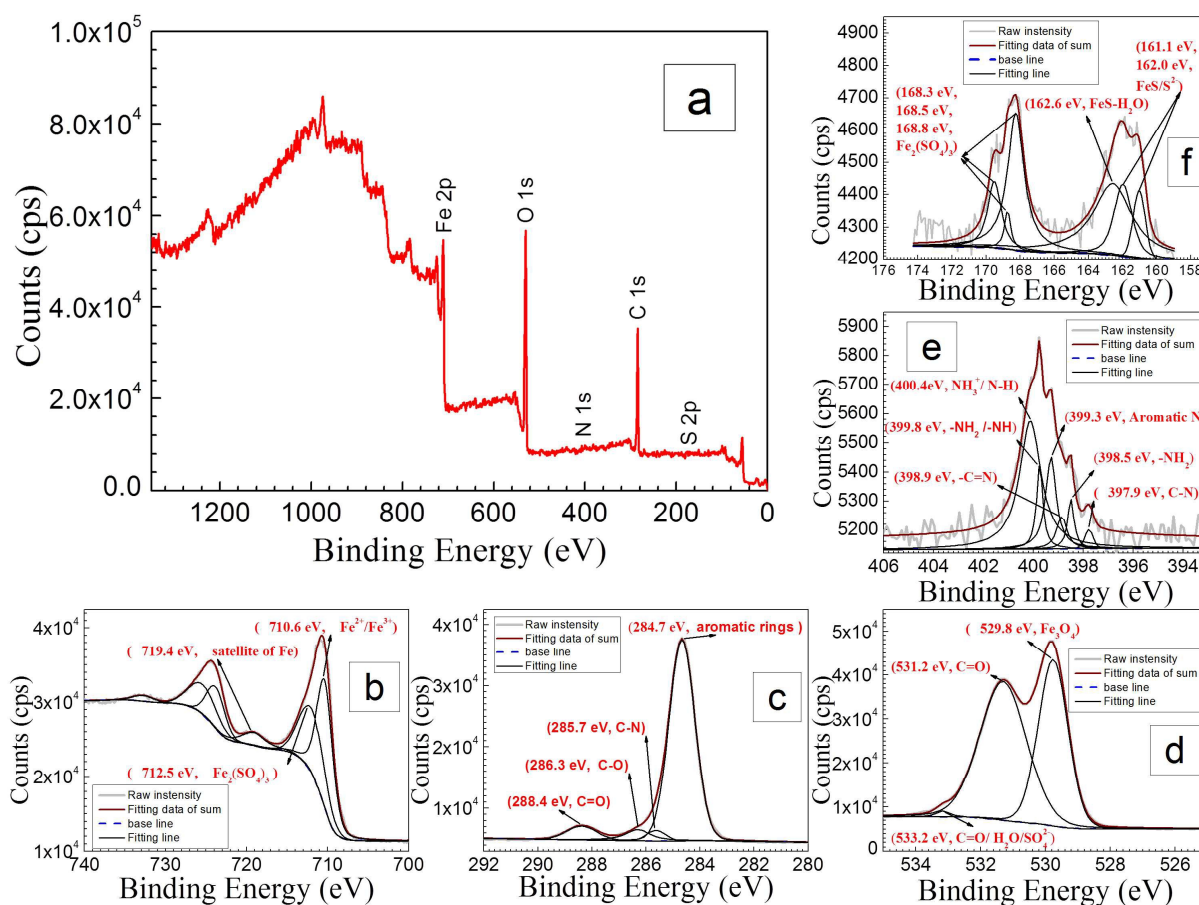


Fig. 8. XPS spectrum for CS surface immersed in 0.5 M HCl with indigo carmine/CTAB inhibitors containing, (a) is the wide-scan spectrum, (b), (c), (d), (e) and (f) are the high-resolution spectrum of Fe 2p, C 1s, O 1s, N 1s and S 2p, respectively.

### 3.4. Theoretical study

#### 3.4.1. Quantum chemical calculations

Quantum chemical calculations were used to investigate the molecular structure property of indigo carmine molecule and other three kinds of cationic organic compound, and estimate the probable adsorption active sites<sup>[23, 55]</sup>. Due to the ionization and protonation, the indigo disulphonate anion of indigo carmine, TEAH of TEA, benzyl trimethyl ammonium cation of BAB and cetyltrimethylammonium cation of CTAB have been calculated by Gaussian 03 software in this study. The frontier molecular orbital surfaces distribution of the optimized molecules were visualized using Gaussian View 5.0 software, and shown in Fig. 9. Some

quantum chemical parameter such as the highest occupied molecular orbital energy ( $E_{\text{HOMO}}$ ), the lowest unoccupied molecular orbital energy ( $E_{\text{LUMO}}$ ), the energy gap ( $\Delta E = E_{\text{LUMO}} - E_{\text{HOMO}}$ ), the absolute electronegativity ( $\chi$ ), global hardness ( $\gamma$ ) and the fraction of the transferred electrons ( $\Delta N$ ) were reported in Table 5.

$E_{\text{HOMO}}$  usually associated the ability of a molecule to donate electrons, and a higher  $E_{\text{HOMO}}$  molecule is more likely to donate electrons to the suitable acceptor with low energy. But, the  $E_{\text{LUMO}}$  associated the ability of a molecule to accept electrons, and a lower  $E_{\text{HOMO}}$  molecule is more likely to accept electrons. The energy gap ( $\Delta E = E_{\text{LUMO}} - E_{\text{HOMO}}$ ), is a significant quantum chemical parameter which represent the adsorption reactivity tendency between a organic molecule and metal surface. And, the adsorption energy will



increase the energy gap ( $\Delta E = E_{\text{LUMO}} - E_{\text{HOMO}}$ ) decreases<sup>[56, 57]</sup>. Fig. 9a and Fig. 9c shows the surfaces of the highest occupied molecular orbital covered on the sulfonic groups of indigo carmine and the nitrogen atom of TEA due to the sulfonic groups and nitrogen atom were well electron-donating groups. This indicated the indigo carmine and TEA molecules could adsorb on the iron surface through a coordination. Due to the ionization of BAB and CTAB molecules in acid solution, the highest occupied molecular orbital covered on the long carbon chain of CTAB and the benzyl group of BAB, not the ammonium group (Fig. 9b and Fig. 9e). It means that the capability of CTAB and BAB to donate electrons were much weaker. Comparing with the TEA and TEAH, we could find the coverage area of highest occupied molecular orbital was change from nitrogen atom to oxygen atoms (Fig. 9c and Fig. 9d). It inferred

us that the protonation could change the molecular hybridization orbital. Table 5 shows that the  $E_{\text{HOMO}}$  of these inhibitor molecules followed in the order of: indigo carmine  $\gg$  TEA  $>$  CTAB  $>$  BAB  $>$  TEAH. It confirm that the capability of donating electrons of these inhibitor molecules followed in the order of indigo carmine  $\gg$  TEA  $>$  CTAB  $>$  BAB  $>$  TEAH. Fig. 9a shows the surfaces of the lowest unoccupied molecular orbital covered on the whole indigo carmine molecule, which means the capability of indigo carmine accepting electrons is much better. But, the  $E_{\text{HOMO}}$  in Table 5 followed in the order of BAB  $>$  TEAH  $>$  CTAB  $\gg$  indigo carmine  $>$  TEA due to the ionization and the protonation of TEA, BAB and CTAB. Consideration of the order of  $\Delta E$  in Table 5 followed in indigo carmine  $<$  CTAB  $<$  BAB  $<$  TEA  $<$  TEAH, which means the adsorption capability of these molecules was indigo carmine  $>$  CTAB  $>$  BAB  $>$  TEA  $>$  TEAH.

Table 5 Quantum chemical parameters calculated using the B3LYP method with a 6-311G(d, p) basis set for indigo disulphonate anion and other cationic organic inhibitors.

Assembly molecules	$E_{\text{HOMO}}$ (eV)	$E_{\text{LUMO}}$ (eV)	$\Delta E$ (eV)	$\mu$ (Debye)	$\chi = (I+A)/2$	$\gamma = (I-A)/2$	$\Delta N$
Indigo carmine	-0.719	1.493	2.212	0.350	-0.387	1.106	3.340
TEA	-5.765	1.844	7.609	3.222	1.960	3.804	0.662
TEAH	-11.349	-3.468	7.881	1.1766	7.409	3.941	-0.052
BAB	-10.364	-4.215	6.148	5.957	7.290	3.074	-0.047
CTAB	-8.956	-3.082	5.874	38.397	6.019	2.937	0.167

According to Koopmans's theorem,  $E_{\text{HOMO}}$  and  $E_{\text{LUMO}}$  are related to the ionization potential ( $I$ ) and the electron affinity ( $A$ ) of the inhibitor molecules and the metal atoms<sup>[58, 59]</sup>, which are estimated by:  $I = -E_{\text{HOMO}}$  and  $A = -E_{\text{LUMO}}$ , respectively<sup>[60]</sup>. Then, the value of  $\chi$  and  $\gamma$  of the inhibitor molecule were calculated from Eq. (17) and Eq. (18)<sup>[61]</sup>:

$$\chi = \frac{I + A}{2} \quad (17)$$

$$\gamma = \frac{I - A}{2} \quad (18)$$

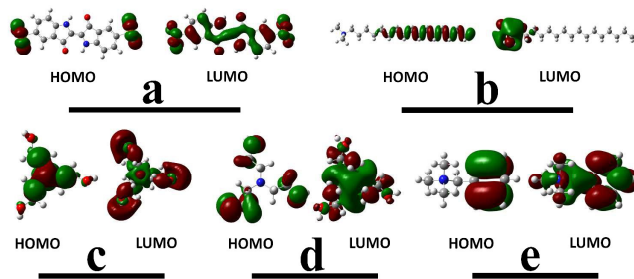


Fig. 9. The frontier molecular orbital ( $E_{\text{HOMO}}$ ,  $E_{\text{LUMO}}$ ) surface for inhibitor molecules, indigo carmine (a), CTAB (b), TEA (c), TEAH (d) and BAB (e).

Thus, the change in the number of electrons transferred ( $\Delta N$ ) is calculated by Eq. (19)<sup>[23, 62]</sup>:

$$\Delta N = \frac{\chi_{\text{Fe}} - \chi_{\text{inh}}}{2(\gamma_{\text{Fe}} + \gamma_{\text{inh}})} \quad (19)$$

where the  $\chi_{\text{Fe}}$  and  $\chi_{\text{inh}}$  are the absolute electronegativity of the iron atom and inhibitor molecules, and the  $\gamma_{\text{Fe}}$  and  $\gamma_{\text{inh}}$  are the global

hardness of the iron atom and inhibitor molecules. In this study, the theoretical values of  $\chi_{\text{Fe}}$  and  $\gamma_{\text{Fe}}$  are taken as 7 eV and 0 eV<sup>[60, 63]</sup>. The calculated results are reported in Table 5. The  $\Delta N$  exhibit the inhibitive performance of the inhibitors resulted from electron donations. If  $\Delta N < 3.6$ , the higher  $\Delta N$  implies higher ability of electrons donations and inhibition efficiency of the inhibitor molecules<sup>[64]</sup>. It can be observed from Table 5 that the  $\Delta N$  of indigo carmine and other three kinds of cationic organic inhibitor molecules to the metal surface follows the order of indigo carmine  $\gg$  TEA  $>$  CTAB  $>$  BAB  $>$  TEAH. Outside the indigo disulphonate anion of indigo carmine which could change the charge of iron surface to negatively and accelerate corrosion, which is in good agreement with the order of the protection efficiency (CTAB  $>$  BAB  $>$  TEA), which most of TEA could protonate to TEAH.

### 3.4.2. Dynamic simulation

Molecular Dynamics simulations have been used to further investigate the adsorption behavior of indigo carmine and other inhibitor molecules on the Fe (1 1 0) surface. The binding energy ( $E_{\text{binding}}$ ) was used to estimate the adsorption intensity of the inhibitor molecules on the Fe (1 1 0) surface when the simulation system reaches thermal and energetic equilibrium. The binding energy in solution simulation system can be calculated by Eq. (20) and Eq. (21):

$$E_{\text{adsorption}} = E_{\text{total}} - (E_{\text{surface+solution}} + E_{\text{inhibitor+solution}}) + E_{\text{solution}} \quad (20)$$

$$E_{\text{binding}} = -E_{\text{adsorption}} \quad (21)$$

where  $E_{\text{total}}$  is the potential energy of the whole simulation system;  $E_{\text{surface+solution}}$  is the potential energies of the simulation system without the inhibitor and  $E_{\text{inhibitor+solution}}$  is the potential energies of the simulation system without the CS surface; and  $E_{\text{solution}}$  is the potential energy of all of the water molecules,  $\text{Cl}^-$  ions and  $\text{H}_3\text{O}^+$  ions. The calculated  $E_{\text{binding}}$ ,  $E_{\text{adsorption}}$  and the maximal experimental inhibition efficiencies of each inhibitors are listed in Table 6. And

the equilibrium configuration of nine kinds simulated system were shown on Fig. 10 and Fig. 11.

Table 6 Binding energies, diffusion coefficient and inhibition efficiencies ( $\eta_{\max}$ ) of indigo carmine and its compound inhibitors.

Inhibitors	$E_{\text{adsorption}}$ (eV)	$E_{\text{binding}}$ (eV)	Diffusion coefficient / ( $10^{-9} \text{m}^2 \text{s}^{-1}$ )		$\eta_{\max}$ (%)
			$\text{H}_3\text{O}^+$	Cl	
indigo carmine	-7.481	7.481	0.13737	0.082842	-202.7
TEA	-3.439	3.439	0.098373	0.123883	39.3
indigo carmine/TEA	-11.333	11.333	0.081077	0.062967	76.4
BAB	-3.220	3.220	0.064103	0.134607	62.1
indigo carmine/BAB	-10.660	10.660	0.06294	0.08728	95.2
CTAB	-1.605	1.605	0.083885	0.090855	97.1
indigo carmine/CTAB	-9.256	9.256	0.04267	0.045315	98.3
TEAH	-3.181	3.181	0.059927	0.134815	--
indigo carmine/TEAH	-10.791	10.791	0.100543	0.061465	--

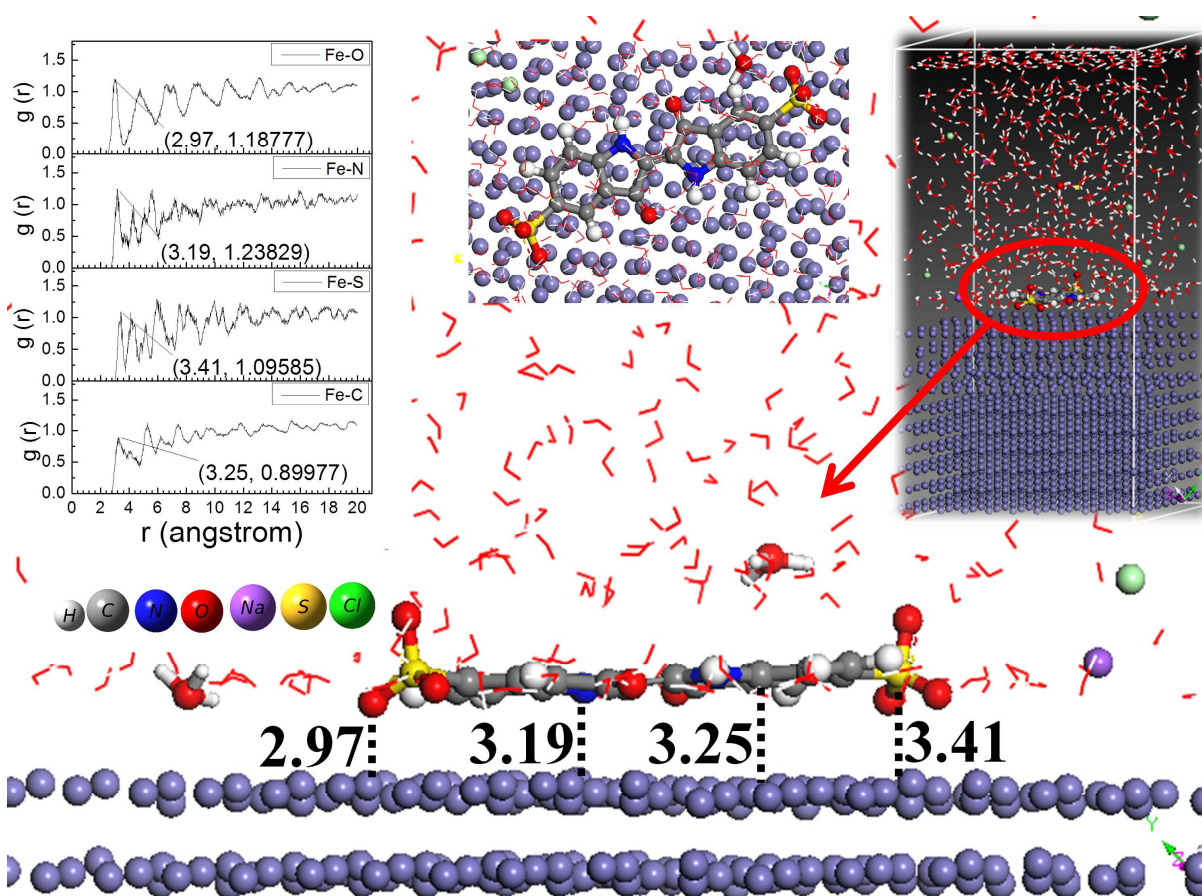


Fig. 10. Equilibrium configuration and most radial distribution function of indigo carmine molecules adsorbed on a Fe (1 1 0) surface

It can be observed from Fig. 10 that the indigo carmine molecule is adsorbed on the the Fe (1 1 0) surface have a planar structure. And the  $E_{\text{binding}}$  of indigo carmine molecule is 7.481 eV (on Table 6), which is much bigger the  $E_{\text{binding}}$  of other three kinds of cationic organic molecules. It means the adsorption capability of indigo carmine molecule is much stronger than other three kinds of

cationic organic molecules. The basic molecule—molecule interaction types can be judged by the typical bonding length. Such as, the typical bond lengths for a van der Waals interaction are 5 Å ~ 10 Å, metal complexation bond lengths are 2 Å ~ 3 Å and H bond lengths are 2 Å ~ 3.5 Å, approximately,<sup>[65, 66]</sup>. In general, the radial distribution function is an effective method to estimate the bond

length. The X position of the first peak always be identified as the bond length, and the peak area is identified as the coordination number. The bond length of chemisorption is within the limits of 1 Å ~ 3.5 Å, while physisorption is longer than 3.5 Å. On the equilibrium configuration of indigo carmine, the radial distribution function of C, N, O and S atoms shows that the bonding length of C-Fe, N-Fe, O-Fe and S-Fe are all less 3.5 Å, especially, the bonding length O-Fe is less 3.0 Å (on Fig. 10). It indicated that all the atoms mentioned above could be coordinately absorbed on the iron surface by donating  $\pi$ -electrons to the unoccupied  $d$ -orbital of iron

to form coordinate bonds, as well as by accepting electrons from  $d$ -orbital of iron to form anti-bonding orbital coordinate bonds<sup>[17, 23, 67]</sup>. In consideration of the frontier molecular orbital of indigo carmine in Fig. 9a, we could infer that the sulfonic acid groups are the main active sites for adsorption between indigo carmine molecule and iron surface, and the existence of indoxyl groups could enhance this adsorption. Thus, we could conclude that the adsorption type of indigo carmine was chemisorptions, and the adsorption intensity is strong.

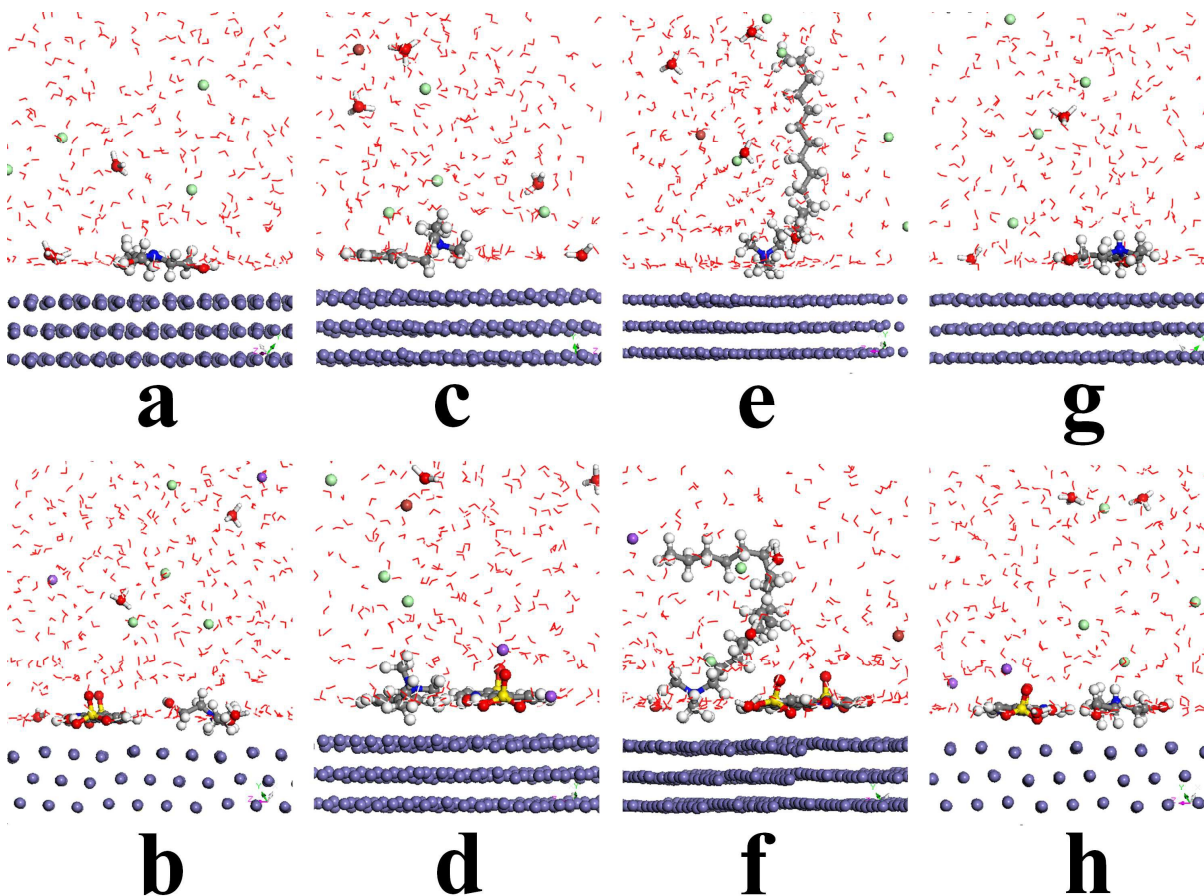


Fig. 11. Equilibrium configuration of cationic organic molecules and their compound inhibitor molecules adsorbed on a Fe (1 1 0) surface, (a) TEA, (b) indigo carmine/TEA, (c) BAB, (d) indigo carmine/BAB, (e) CTAB, (f) indigo carmine/CTAB, (g) TEAH and indigo carmine/TEAH.

From Fig. 11, we can find most the cationic organic molecules and their compound inhibitor molecules are adsorbed on the Fe (1 1 0) surface have a planar structure (Fig. 11a, Fig. 11c and Fig. 11g.). the CTAB molecules is adsorbed on the Fe (1 1 0) surface have a vertical structure due to the long-chain structure of CTAB is a hydrophobic group. In addition, the  $E_{\text{binding}}$  of single inhibitor molecules are followed in the order of indigo carmine  $\gg$  TEA  $>$  BAB  $>$  TEAH  $>$  CTAB (on Table 6). Except the CTAB, this order of  $E_{\text{binding}}$  is consistent with the order of the  $\Delta N$  of indigo carmine and other three kinds of cationic organic inhibitor molecules (indigo carmine  $\gg$  TEA  $>$  CTAB  $>$  BAB  $>$  TEAH). The reason may be that the CTAB molecule can be adsorbed on iron surface by its amino group not the long carbon chain, but the surfaces of the highest occupied molecular orbital covered on the long carbon group. Comparing the equilibrium configuration of TEA and TEAH, the protonated amino

groups,  $[-\text{NH}_2\text{-R}]^+$ , was not adsorbed on iron surface (on Fig. 11a and Fig. 11g), possible because of the electron-deficient nature of the protonated N atom. Thus the  $E_{\text{binding}}$  of TEAH molecule is smaller than TEA molecule. In additionally, the partial TEA molecule could combine with indigo carmine molecule due to the electrostatic attraction between sulfonate group and H atom present in hydroxyl group of TEA molecule. Thus, the partial TEAH molecules of TEAH/indigo carmine compound inhibitors will be replaced by the TEA molecules. That means the effect of TEAH molecule adsorption on CS surface for keeping the balance of charge will not well due to the competitive adsorption of TEA molecule. That is why the inhibition effect of indigo carmine/TEA compound inhibitor is not well. In order to analyze the synergy between the indigo carmine molecule and cationic organic molecule, we have compared the  $E_{\text{binding}}$  between the compound inhibitors and single inhibitors on Table 6. we can find the  $E_{\text{binding}}$  of the compound inhibitors is bigger



than the sum of the  $E_{\text{binding}}$  of single inhibitors (such as  $E_{\text{binding}}$  of indigo carmine/TEA is bigger than sum of the  $E_{\text{binding}}$  of single indigo carmine molecule and single TEA). It means that the adsorption

capability of compound inhibitors can be enhanced by synergistic effect.

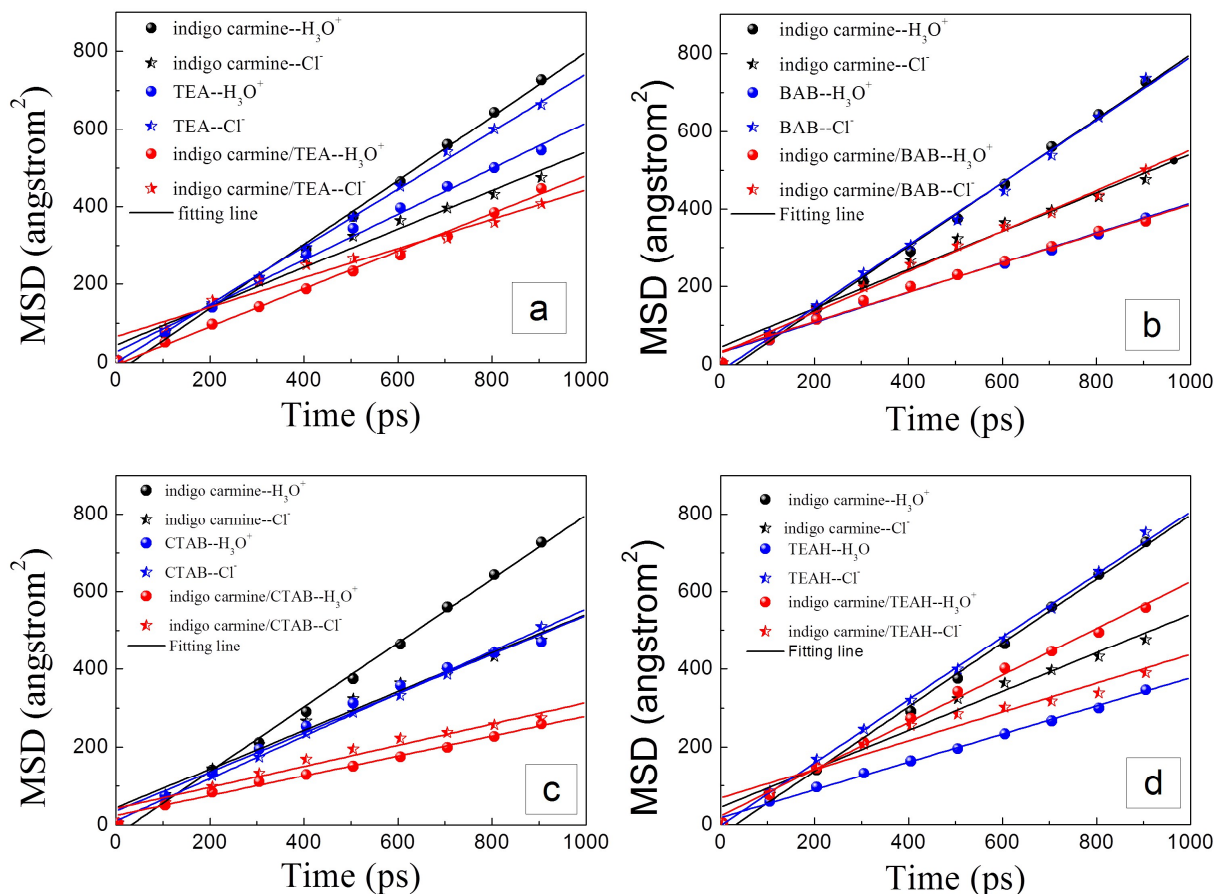


Fig. 12. Time evolution of mean square displacements of corrosive species ( $\text{H}_3\text{O}^+$  ions and  $\text{Cl}^-$  ions) in all the dynamic simulations system, (a) indigo carmine/TEA and TEA systems, (b) indigo carmine/BAB and BAB systems, (c) indigo carmine/CTAB and CATB systems and (d) indigo carmine/TEAH and TEAH systems.

In order to investigate the synergistic mechanism of indigo carmine and cationic organic compound inhibitors by molecular dynamics simulation, the diffusion coefficient ( $D$ ) of can be used to describe the migration rate of a corrosive species ( $\text{H}_3\text{O}^+$  ions and  $\text{Cl}^-$  ions) in simulation system. A small diffusion coefficient means strong hinder of simulation system and weak reactivity of  $\text{H}_3\text{O}^+$  ions and  $\text{Cl}^-$  ions, which will induce to high inhibition efficiency. The diffusion coefficient is defined as follow<sup>[66, 68, 69]</sup>:

$$MSD(t) = \left[ \frac{1}{N} \sum_{i=1}^N |R_i(t) - R_i(0)|^2 \right] \quad (22)$$

$$D = \frac{1}{6} \lim_{t \rightarrow \infty} \frac{d}{dt} \sum_i^N \left[ |R_i(t) - R_i(0)|^2 \right] \quad (23)$$

where  $N$  is the number of target molecules  $|R_i(t) - R_i(0)|^2$  is the mean-square displacement (MSD),  $R_i(t)$  and  $R_i(0)$  are positions of corrosive species at time  $t$  and 0, respectively. The MSD plots was showed on Fig. 12. The calculated diffusion coefficients of  $\text{H}_3\text{O}^+$  ions and  $\text{Cl}^-$  ions in dynamic simulations system are shown in Table 6.

From the Fig.12 and Table 6, we can find the  $D$  of  $\text{H}_3\text{O}^+$  ions and  $\text{Cl}^-$  ions in compound inhibitors simulation system is smaller than the  $D$  of  $\text{H}_3\text{O}^+$  ions in single indigo carmine inhibitor simulation system and the  $D$  of  $\text{Cl}^-$  ions in single cationic organic inhibitors. It means the migration rate of a corrosive species ( $\text{H}_3\text{O}^+$  ions and  $\text{Cl}^-$  ions) in simulation system are both be inhibited by the indigo disulphonate anion and other organic cation being simultaneously adsorbed on iron surface and balancing the charge of iron surface.

Also, we have investigated the surface concentration profiles of corrosive species ( $\text{H}_3\text{O}^+$  ions and  $\text{Cl}^-$  ions) in the dynamic simulations system which on the normal direction (0 0 1), and the results are shown in Fig. 13. It can be observed from Fig. 13 that the  $\text{H}_3\text{O}^+$  ions and  $\text{Cl}^-$  ions distribution of compound inhibitors simulation system are farther from the iron surface than the  $\text{H}_3\text{O}^+$  ions and  $\text{Cl}^-$  ions distribution of single indigo carmine simulation system and single cationic organic inhibitors simulation system, respectively. It means that the compound inhibitors of indigo carmine and cationic organic inhibitors could balance the charge of iron surface, and keep the corrosive species ( $\text{H}_3\text{O}^+$  ions and  $\text{Cl}^-$  ions) away from the iron surface. Thus, we can conclude that the indigo

carmine could cooperate with the cationic organic compounds to synergistically inhibit the corrosion of iron in 0.5 M HCl solution.

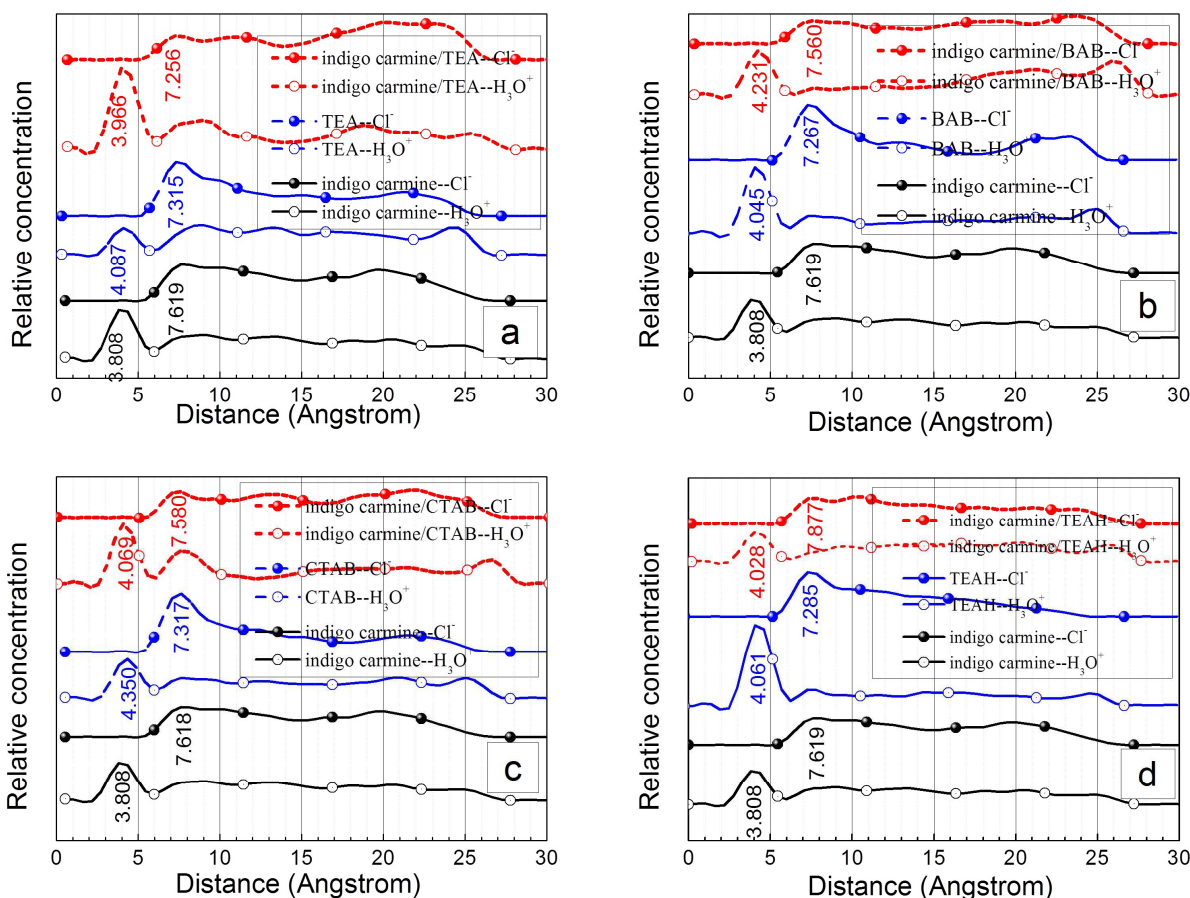


Fig. 13. Surface concentration of corrosive species (H<sub>3</sub>O<sup>+</sup> ions and Cl<sup>-</sup> ions) in all the dynamic simulations system, all are on the normal direction (0 0 1), (a) indigo carmine/TEA and TEA systems, (b) indigo carmine/BAB and BAB systems, (c) indigo carmine/CTAB and CTAB systems and (d) indigo carmine/TEAH and TEAH systems.

#### 4. Conclusions

This study demonstrated a superior synergistic inhibition effect between the indigo carmine and three kinds of cationic organic compounds. The results confirmed that the indigo disulphonate ions of indigo carmine molecule could adsorb strongly on CS surface, but it is unable to protect the iron from corrosion due to the negatively charged surface. However, the indigo carmine cooperating with cationic organic compounds could effectively inhibit the CS from corrosion in 0.5 M HCl solution, for the indigo disulphonate anion and organic cation were simultaneously adsorbed on the CS surface to balance the charge distribution of CS surface. And the indigo carmine/BAB compound inhibitor showed the best synergistic inhibition effect ( $S=17.14$ ), and the best inhibition efficiency of them is 95.0%. Due to the hydrophobicity of CTAB, the indigo carmine/CTAB compound inhibitor showed the best inhibition effect ( $\eta = 98.5\%$ ) at the concentration of  $5 \times 10^{-5}$  M.

The corrosion morphology of each SEM samples and XPS spectra corroborated the electrochemical measurements and showed evidence of the chemisorptions of indigo carmine and three

kinds of cationic organic compounds on the CS surface. And the micrograph feature of micro-cracks and porous may be used to distinguish the hydrogen evolution corrosion and pitting corrosion of Cl<sup>-</sup> ions, respectively.

In additionally, the investigation of quantum chemical calculations and molecular dynamics simulation adequately confirmed the indigo carmine could cooperate with the cationic organic compounds to synergistically inhibit the corrosion of iron in 0.5 M HCl solution. The diffusion coefficient and the surface concentration profile would be a useful method to investigate the synergistically inhibition effect in acid solution.

#### Acknowledgements

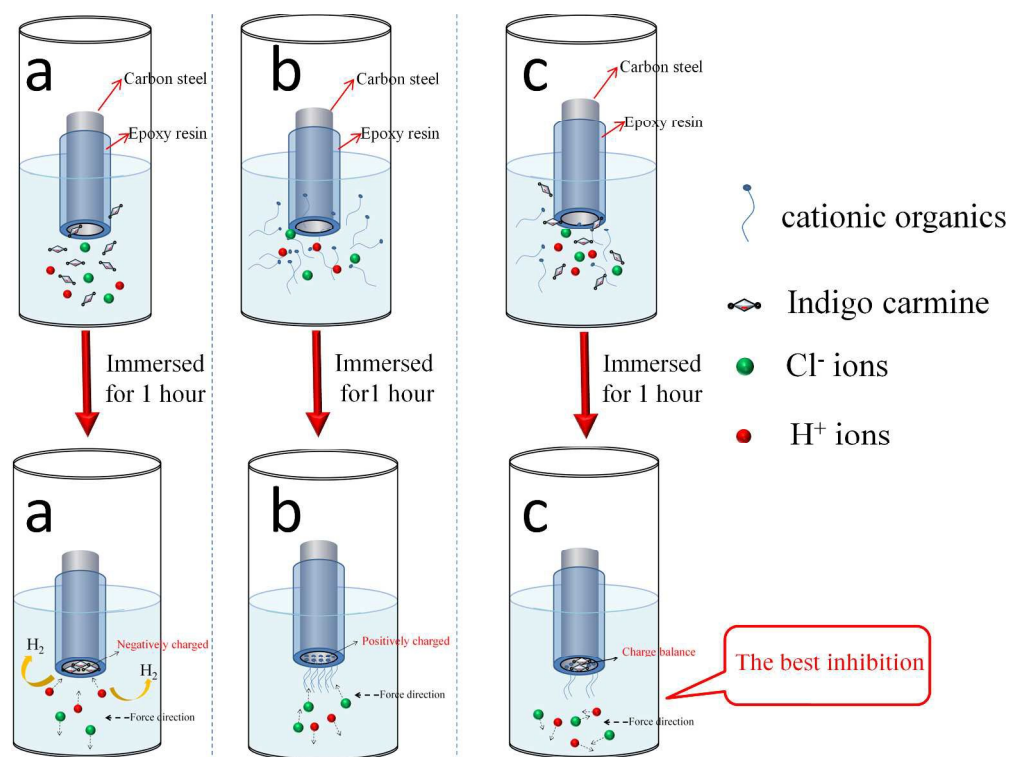
This work was funded by Guangxi Natural Science Foundation (2013GXNSFBA 019248) and the Research Fund for the Guangxi Higher Education (2013YB114).

#### References

1. B. Zhang, C. He, C. Wang, P. Sun, F. Li and Y. Lin, *Corrosion*

- Science, 2014. (<http://dx.doi.org/10.1016/j.corsci.2014.10.054>)
2. N. Soltani, M. Behpour, E. E. Oguzie, M. Mahluji and M. A. Ghasemzadeh, *RSC Adv.*, 2015, **5**, 11145-11162.
  3. I. B. Obot, E. E. Ebenso and M. M. Kabanda, *Journal of Environmental Chemical Engineering*, 2013, **1**, 431-439.
  4. P. Roy, T. Maji, S. Dey and D. Sukul, *RSC Adv.*, 2015, **5**, 61170-61178.
  5. S. A. Umoren and M. M. Solomon, *Journal of Industrial and Engineering Chemistry*, 2015, **21**, 81-100.
  6. E. E. Ebenso and E. E. Oguzie, *Materials Letters*, 2005, **59**, 2163-2165.
  7. E. E. Oguzie, B. N. Okolue, C. E. Ogukwe and C. Unaegbu, *Materials Letters*, 2006, **60**, 3376-3378.
  8. Y. Abboud, A. Abourriche, T. Saffaj, M. Berrada, M. Charrouf, A. Bennamara and H. Hannache, *Desalination*, 2009, **237**, 175-189.
  9. A. Singh, Y. Lin, W. Liu, S. Yu, J. Pan, C. Ren and D. Kuanhai, *Journal of Industrial and Engineering Chemistry*, 2014, **20**, 4276-4285.
  10. E. E. Oguzie, C. Unaegbu, C. N. Ogukwe, B. N. Okolue and A. I. Onuchukwu, *Materials Chemistry and Physics*, 2004, **84**, 363-368.
  11. M. Abdeli, N. P. Ahmadi and R. A. Khosroshahi, *Journal of Solid State Electrochemistry*, 2009, **14**, 1317-1324.
  12. Z. Zhang, N. C. Tian, X. Y. Li, L. Zhang, L. Wu and Y. Huang, *Applied Surface Science*, 2015, **357**, 845-855.
  13. R. E. Melchers, *Corrosion Science*, 2003, **45**, 2609-2625.
  14. Y. Y. Chen, H. J. Tzeng, L. I. Wei, L. H. Wang, J. C. Oung and H. C. Shih, *Corrosion Science*, 2005, **47**, 1001-1021.
  15. S. P. Li, J. Guo, S. W. Yang, X. L. He, *Journal of University of Science and Technology Beijing*, 2008, **30**, 16-20. (In Chinese)
  16. H.Y. Mao, Q. W. Cai, H. B. Wu, C. F. Sun, J. M. Liang, *Corrosion & Protection*, 2013, **34**, 499-502. (In Chinese)
  17. Z. Zhang, N. Tian, L. Zhang and L. Wu, *Corrosion Science*, 2015.
  18. M. J. Frisch, G. W. Trucks, H. B. Schlegel, G. E. Scuseria, M. A. Robb, J. R. Cheeseman, J. A. Montgomery, Jr., T. Vreven, K. N. Kudin, J. C. Burant, J. M. Millam, S. S. Iyengar, J. Tomasi, V. Barone, B. Mennucci, M. Cossi, G. Scalmani, N. Rega, G. A. Petersson, H. Nakatsuji, M. Hada, M. Ehara, K. Toyota, R. Fukuda, J. Hasegawa, M. Ishida, T. Nakajima, Y. Honda, O. Kitao, H. Nakai, M. Klene, X. Li, J. E. Knox, H. P. Hratchian, J. B. Cross, C. Adamo, J. Jaramillo, R. Gomperts, R. E. Stratmann, O. Yazyev, A. J. Austin, R. Cammi, C. Pomelli, J. W. Ochterski, P. Y. Ayala, K. Morokuma, G. A. Voth, P. Salvador, J. J. Dannenberg, V. G. Zakrzewski, S. Dapprich, A. D. Daniels, M. C. Strain, O. Farkas, D. K. Malick, A. D. Rabuck, K. Raghavachari, J. B. Foresman, J. V. Ortiz, Q. Cui, A. G. Baboul, S. Clifford, J. Cioslowski, B. B. Stefanov, G. Liu, A. Liashenko, P. Piskorz, I. Komaromi, R. L. Martin, D. J. Fox, T. Keith, M. A. Al-Laham, C. Y. Peng, A. Nanayakkara, M. Challacombe, P. M. W. Gill, B. Johnson, W. Chen, M. W. Wong, C. Gonzalez, and J. A. Pople, Gaussian, Inc., Wallingford CT, 2004.
  19. A.D. Becke, *Phys. Rev. A*, 1988, **38**, 3098-3100.
  20. C. Lee, W. Yang, R.G. Parr, *Phys. Rev.*, 1988, **37**, 785-789.
  21. A.D. Becke,; Density-functional thermochemistry. III. The role of exact exchange, *J. Chem. Phys.*, 1993, **98**, 5648-5652.
  22. Materials Studio, Revision 6.0, Accelrys Inc., San Diego, USA, 2011.
  23. H. Zhao, X. Zhang, L. Ji, H. Hu and Q. Li, *Corrosion Science*, 2014, **83**, 261-271.
  24. M. A. Amin, K. F. Khaled, Q. Mohsen and H. A. Arida, *Corrosion Science*, 2010, **52**, 1684-1695.
  25. Y. Tang, L. Yao, C. Kong, W. Yang and Y. Chen, *Corrosion Science*, 2011, **53**, 2046-2049.
  26. M. A. Deyab, *International Journal of Hydrogen Energy*, 2013, **38**, 13511-13519.
  27. S. Thomas, N. V. Medhekar, G. S. Frankel and N. Birbilis, *Current Opinion in Solid State and Materials Science*, 2015, **19**, 85-94.
  28. M. A. Deyab, *Journal of Power Sources*, 2013, **242**, 86-90.
  29. R. Solmaz, E. Altunbaş and G. Kardaş, *Materials Chemistry and Physics*, 2011, **125**, 796-801.
  30. A. Yousefi, S. Javadian, N. Dalir, J. Kakemam and J. Akbari, *RSC Adv.*, 2015, **5**, 11697-11713.
  31. M. A. Deyab, *Journal of Power Sources*, 2014, **268**, 765-770.
  32. F. Bentiss, M. Lebrini and M. Lagrenée, *Corrosion Science*, 2005, **47**, 2915-2931.
  33. X. Li, S. Deng and X. Xie, *Corrosion Science*, 2014, **81**, 162-175.
  34. H. Ashassi-Sorkhabi and E. Asghari, *Electrochimica Acta*, 2008, **54**, 162-167.
  35. B. D. Mert, A. O. Yüce, G. Kardaş and B. Yazıcı, *Corrosion Science*, 2014, **85**, 287-295.
  36. B. Hirschorn, M. E. Orazem, B. Tribollet, V. Vivier, I. Frateur and M. Musiani, *Journal of The Electrochemical Society*, 2010, **157**, C458.
  37. B. Hirschorn, M. E. Orazem, B. Tribollet, V. Vivier, I. Frateur and M. Musiani, *Electrochimica Acta*, 2010, **55**, 6218-6227.
  38. .
  39. E. A. Flores, O. Olivares, N. V. Likhanova, M. A. Domínguez-Aguilar, N. Nava, D. Guzman-Lucero and M. Corrales, *Corrosion Science*, 2011, **53**, 3899-3913.
  40. A. A. Hermas and M. S. Morad, *Corrosion Science*, 2008, **50**, 2710-2717.
  41. E. McCafferty, N. Hackerman, *Electrochem. Soc.*, 1972, **119**, 146-154.
  42. E. McCafferty, Introduction to Corrosion Science, *Springer, New York, Dordrecht, Heidelberg, London, New York*, 2010.
  43. A. Kosari, M. H. Moayed, A. Davoodi, R. Parvizi, M. Momeni, H. Eshghi and H. Moradi, *Corrosion Science*, 2014, **78**, 138-150.
  44. M. K. Pavithra, T. V. Venkatesha, M. K. Punith Kumar and H. C. Tondan, *Corrosion Science*, 2012, **60**, 104-111.
  45. M. Finšgar, *Corrosion Science*, 2013, **72**, 82-89.
  46. A. El Bribri, M. Tabyaoui, B. Tabyaoui, H. El Attari and F. Bentiss, *Materials Chemistry and Physics*, 2013, **141**, 240-247.
  47. M. A. Abu-Dalo, N. A. F. Al-Rawashdeh and A. Ababneh, *Desalination*, 2013, **313**, 105-114.
  48. S. Kallip, A. C. Bastos, K. A. Yasakau, M. L. Zheludkevich and M. G. S. Ferreira, *Electrochemistry Communications*, 2012, **20**, 101-104.
  49. S. Munktel, M. Tydén, J. Högström, L. Nyholm and F. Björefors, *Electrochemistry Communications*, 2013, **34**, 274-277.
  50. F. El-Taib Heakal, O. S. Shehata, N. S. Tantawy and A. M. Fekry, *International Journal of Hydrogen Energy*, 2012, **37**,

- 84-94.
51. Z. Zhang, S. Chen, Y. Li, S. Li and L. Wang, *Corrosion Science*, 2009, **51**, 291-300.
  52. A. Alagta, I. Felhósi, I. Bertoti and E. Kálmán, *Corrosion Science*, 2008, **50**, 1644-1649.
  53. <http://www.lasurface.com/database/elementxps.php> (12/10/2015).
  54. <http://srdata.nist.gov/xps/Default.aspx> (12/10/2015)
  55. R. Yıldız, *Corrosion Science*, 2015, **90**, 544-553.
  56. L. Herrag, B. Hammouti, S. Elkadiri, A. Aouniti, C. Jama, H. Vezin and F. Bentiss, *Corrosion Science*, 2010, **52**, 3042-3051.
  57. I. B. Obot and N. O. Obi-Egbedi, *Corrosion Science*, 2010, **52**, 198-204.
  58. H. Tian, W. Li, K. Cao and B. Hou, *Corrosion Science*, 2013, **73**, 281-291.
  59. M. A. Hegazy, A. M. Badawi, S. S. Abd El Rehim and W. M. Kamel, *Corrosion Science*, 2013, **69**, 110-122.
  60. F. Zhang, Y. Tang, Z. Cao, W. Jing, Z. Wu and Y. Chen, *Corrosion Science*, 2012, **61**, 1-9.
  61. K. Zhang, B. Xu, W. Yang, X. Yin, Y. Liu and Y. Chen, *Corrosion Science*, 2015, **90**, 284-295.
  62. G. Xia, X. Jiang, L. Zhou, Y. Liao, M. duan, H. Wang, Q. Pu and J. Zhou, *Corrosion Science*, 2015.
  63. A. Kokalj, *Chemical Physics*, 2012, **393**, 1-12.
  64. H. Ju, Z.-P. Kai and Y. Li, *Corrosion Science*, 2008, **50**, 865-871.
  65. A. Kühnle, *Current Opinion in Colloid & Interface Science*, 2009, **14**, 157-168.
  66. Z. Xu, S.-L. Yuan, H. Yan and C.-B. Liu, *Colloids and Surfaces A: Physicochemical and Engineering Aspects*, 2011, **380**, 135-142.
  67. Z. Cao, Y. Tang, H. Cang, J. Xu, G. Lu and W. Jing, *Corrosion Science*, 2014, **83**, 292-298.
  68. Y. Yan, X. Wang, Y. Zhang, P. Wang, X. Cao and J. Zhang, *Corrosion Science*, 2013, **73**, 123-129.
  69. A. Guo, G. Duan, K. He, B. Sun, C. Fan and S. Hu, *Computational and Theoretical Chemistry*, 2013, **1015**, 21-26.



254x190mm (300 x 300 DPI)